NOAA Technical Memorandum ERL NSSL-79

SUBSYNOPTIC SCALE DYNAMICS AS REVEALED BY USE OF FILTERED SURFACE DATA

Charles A. Doswell III*

National Severe Storms Laboratory
Norman, Oklahoma
December 1976

Property of
NWC Library
University of Oklahoma

*Present Affiliation:
National Severe Storms Forecast Center
NOAA National Weather Service
Kansas City, Missouri

UNITED STATES
DEPARTMENT OF COMMERCE
Elliot L. Richardson, Secretary

NATIONAL OCEANIC AND
ATMOSPHERIC ADMINISTRATION
Robert M. White, Administrator

Environmental Research
Laboratories
Wilmot N. Hess, Director

TABLE OF CONTENTS

LIST OF FIGURES

LIST OF SYMBOLS

Note: Except where otherwise noted, an asterisk (*) denotes the dimensional form of a variable.

ROMAN SYMBOLS

C	condensation rate
c_p	specific heat at constant pressure
D	spatial weight function parameter; characteristic depth scale
$\hat{e}$	unit vector
f	Coriolis parameter
$\vec{F}$	frictional force vector
f_o	characteristic Coriolis parameter
Fr	Froude number
g	acceleration of gravity
H	scale height of the atmosphere
$\tilde{H}$	turbulent heat flux
k^*,k	wavenumber
$\hat{k}$	unit vector in the vertical
L^*,L	wavelength; characteristic horizontal length scale; latent heat of condensation
N	temporal weight function parameter
N_1^*,N_2^*	pseudo-random numbers (asterisk convention does not apply)
p	pressure
p^*	period
p_Δ	minimum resolvable period
Q	diabatic heating rate
r	response function; mixing ratio
R^*,R	radius from observation point to grid point

Ri	Richardson Number
Ro	Rossby number
T*,T	time separation of observation from grid point; temperature
u	eastward wind component
v	northward wind component
V	characteristic horizontal velocity amplitude
$\vec{V}$	horizontal wind vector
$\tilde{w}$	weight function
w	vertical wind component
W	characteristic vertical velocity amplitude
$\vec{x}$	position vector
x_o,y_o	coordinates of uniformly distributed grid points
x_r,y_r	coordinates of pseudo-randomly distributed grid points
$\vec{Y}$	weighted position vector

GREEK SYMBOLS

α	specific volume
β	number of temporal grid intervals at the characteristic value of T*
$\delta r,\Delta r$	differences in low-pass response at center of band
δ	horizontal divergence
$\delta(\ )$	a finite difference
Δs	Spatial grid interval
Δt	temporal grid interval
ζ	vertical component of vorticity
η	temporal weight function parameter-dimensional; friction coefficient
θ	potential temperature
κ	spatial weight function parameter-dimensional

λ	ratio of wavelength to spatial grid interval
ν^*, ν	frequency
ρ	number of spatial grid intervals at the characteristic value of R*
σ	image scale factor
σ_s	standard atmosphere lapse rate parameter
τ	characteristic time scale; ratio of period to temporal grid interval
ϕ	general variable
ϕ_{ijk}	filtered value of ϕ at the grid point $x = x_o + i\Delta s, \quad y = y_o + j\Delta s, \quad t = t_o + k\Delta t$
Φ	characteristic value for ϕ

SPECIAL SYMBOLS

∇	horizontal gradient operator
$( )_a$ or $( )^{(a)}$	low-pass value from filter with least response
$( )_b$ or $( )^{(b)}$	low-pass value from filter with most response
$( )_L$	large scale component
$( )_M$	medium scale component
$( )_S$	small scale component
$( )_s$	spatial domain
$( )_t$	temporal domain
$( )'$	perturbation quantity

Where a variable name has more than one definition, the second is separated from the first by a semicolon. The meaning should be clear from the context.

SUBSYNOPTIC SCALE DYNAMICS AS REVEALED BY USE OF FILTERED SURFACE DATA

Charles A. Doswell III

A band-pass filtering technique, based on an exponential weight function interpolation method, is presented. Both spatial and temporal filtering are simultaneously accomplished and the center of the band can be positioned within the spectral domain to satisfy user needs. The filter is applied to conventional surface meteorological observations for eight severe thunderstorm days in Oklahoma. Surface subsynoptic systems are shown to be well correlated with severe weather events.

Combining results of the filtering with available numerical studies permits a scale analysis for subsynoptic systems. Three fundamental findings about these systems are developed: first, the data support the hypothesis that the circulations derive their energy from baroclinic sources; second, anisentropic processes of eddy mixing and latent heat release are apparently vital to the subsynoptic flow; and third, evidence supports the existence of a balance between pressure forces and momentum transport via vertical circulations. Those findings are in basic agreement with previous medium-scale dynamical theory and experiment, but the lack of information about vertical structure precludes a definitive description of subsynoptic circulations.

1. INTRODUCTION

Observation and analysis of a phenomenon are the first steps in the development of most meteorological concepts. Unlike modern physics, where theory frequently precedes observation[1], meteorological concepts have typically developed after a long series of observations followed by the abstraction of the relevant physical concept. Recent meteorological theory consistently emphasizes the concept of a phenomenon's scale (e.g., Palmén and Newton, 1969) in an effort to separate meaning from "noise". Unfortunately, there is no general agreement on definition of those scales. Meteorological phenomena generally operate over a range of values for the scaling parameters. As a result, a particular phenomenon may occur in that part of the range overlapped by another and when scale limits are set arbitrarily in this overlap region, neither phenomenon has an unambiguous scale. We generally assign arbitrary limits to small (micro), medium (meso), and large (macro) scales, but these are only rough guidelines. A purpose for doing so is to eliminate those events which have relatively insignificant effects.

[1] As an example, the prediction of the existence of sub-nuclear particles based on theoretical evidence has typically preceded actual observation of the particles.

Scale definition is complicated by the lack of an information theory for meteorological observations such as exists for pure time series observations (see Blackman and Tukey, 1958). Meteorological data involve both spatial and temporal sampling. Since meteorological waves travel and evolve in space and time, further complications are introduced. By using the time series observations available at the fixed locations of our network (see Amble, 1953), analysis should be improved. However, it is not clear how this is to be accomplished most effectively.

Much meteorological analysis is empirical or heuristic. In fact, the subject of objective analysis is largely concerned with interpolation and the methods used can be only subjectively justified since the "true" fields are unknown. Gandin's work (1963) attempts to clarify interpolation error effects based on correlation functions developed for data ensembles. The variational methods of Sasaki (1958, 1970) may be thought of as a filtering technique based in part on physical constraints. Stephens (1971) has pointed out that physical constraints involving observed derivatives can reduce aliasing by effectively decreasing the Nyquist interval. Methods based on physics hold great promise for extending the utility of meteorological analysis. One must have some prior knowledge of the physics to apply such constraints, however.

One scale of meteorological phenomena which remains poorly observed and, hence, poorly understood is the so-called mesoscale. For our purposes, mesoscale motions encompass phenomena whose spatial dimensions are 10 to 10^3 km, and whose temporal dimensions range from 1 hr to 10 hr. Sampling theory suggests the upper limits of the mesoscale range are sampled more or less adequately by the conventional surface station network of reporting stations operated by the National Weather Service in cooperation with the Federal Aviation Administration. It is within the mesoscale range that there exists a so-called "spectral gap" (see Lumley and Panofsky, 1964). That is, the time averaged power in that part of the spectrum is generally much less than at larger and smaller scales. However, it is also within this range that the relatively rare (but exceedingly important) severe local storm occurs.

Individual severe storms and their attendant effects are at the lower mesoscale range and thus are not adequately sampled by the conventional network. But these storms tend to occur in ways which indicate organization on a larger scale (Tegtmeier, 1974; McFarland, 1975) and yet this larger scale is not as large as the extratropical cyclone (synoptic) scale. The question is whether subsynoptic scale systems exist that can be resolved by the conventional data network. Provided that such systems exist, they must be observed enough times to allow abstraction of the relevant physical concepts--i.e., their dynamics.

To isolate phenomena of the scale considered, a band-pass filtering technique is proposed. A band-pass filter is one which reduces amplitudes at scales below and above the one of interest. Variational band-pass filters have been developed by Hylton (1972) and Sheets (1972). Hylton's band-pass filter is designed to limit the magnitude of derivatives of the analyzed fields but includes no model constraints. Sheets treats the tropical cyclone and incorporates derivative filters like those of Hylton with a simple model applicable to tropical cyclones.

The state of knowledge concerning the subsynoptic scale is sketchy, at best. Tegtmeier (1974) has indicated, via subjective analysis, some of the types of subsynoptic systems that occur in the Great Plains. Matsumoto, Ninomiya, and Akayama (1967) present a case study of a subsynoptic system and Matsumoto and Ninomiya (1969) propose one theoretical model that may be applicable. Sasaki (1973) presents some provocative results concerning momentum fluxes based on variational analysis of surface data for a case study in Oklahoma. McGinley and Sasaki (1975) have proposed that symmetric baroclinic instabilities may be present in severe storm generating systems. The model of Matsumoto and Ninomiya (1969) proposes an interaction between gravitational modes and "synoptic" modes. There have been proposals (Maddox and Gray, 1973) that CISK (forced Ekman boundary layer pumping, described by Charney and Eliassen, 1964) may have some crucial role. Nevertheless, there is not enough observational knowledge of the four-dimensional structure of subsynoptic systems to allow any single model to emerge as the basic physical mechanism.

In spite of deficiencies in understanding events on the subsynoptic scale, some problems can be resolved by the technique of band-pass filtering. By designing the filter to isolate subsynoptic scale features, characteristic values can be estimated for variables of interest. When these values are established, a scale analysis appropriate to the subsynoptic range can be done. This scale analysis is tentative, owing to lack of information about the vertical structure. However, results of numerical simulations and theoretical studies can be used to supplement the surface observations; thus, dynamical insights can be gained into subsynoptic systems and their role in severe convective storms.

2. FILTERING TECHNIQUE

2.1 The Barnes Interpolation Scheme

The basic tool used throughout this analysis is the interpolation scheme developed by Barnes (1964, 1973). Although any interpolation scheme could be used to develop a band-pass filter, Barnes' method is particularly convenient, owing to the simple functional form of the weight functions. This method is of the weighted-average type, with the weight function given by

$$\tilde{w}\,(\vec{x}) = \exp\,[-\vec{Y} \cdot \vec{Y}]\ , \tag{1}$$

where $\vec{x}$ is the position vector given by

$$\vec{x} = (x_1\hat{e}_1 + x_2\hat{e}_2 + \ldots + x_n\hat{e}_n)\ ,$$

and $\vec{Y}$ is the weighted position vector

$$\vec{Y} = \left[\frac{x_1}{2(\kappa_1)^{1/2}}\,\hat{e}_1 + \frac{x_2}{2(\kappa_2)^{1/2}}\,\hat{e}_2 + \ldots + \frac{x_n}{2(\kappa_n)^{1/2}}\,\hat{e}_n\right] \quad ,$$

and the $\hat{e}_i$ are the n unit vectors in the n-dimensional space over which the analysis is applied. Consider a weight function which is isotropic and homogeneous in x-y space, so that the spatial coordinate is simply the distance from the grid point to the data point in question. The second coordinate is the temporal separation. Thus, (1) is simply

$$\tilde{w}\ (R^*,\ T^*;\ \kappa,\ \eta) = \exp\left[-\frac{R^{*2}}{4\kappa} - \frac{T^{*2}}{4\eta}\right] \quad , \tag{2}$$

where R* and T* are the dimensional distance and time separation, and κ and η are the distance and time parameters at our disposal for weighting specification.

Barnes has shown that interpolation using (2) acts as a low-pass filter with a particularly simple response function:

$$r\ (\ k^*,\ \nu^*;\ \kappa,\ \eta) = \exp\left[-\kappa k^{*2} - \eta\nu^{*2}\right] \quad , \tag{3}$$

where k* and ν* are the dimensional wavenumber and frequency. Owing to the smooth nature of the weight function, the response is also smooth and problems associated with side lobes (Sasaki, 1960) are avoided.

Application of this interpolation method is to filter the data. Thus, it is not desirable accurately to reproduce input observations at all points in space and time. Results are expected to depart from the observations, especially in areas affected by thunderstorm-induced flows. Only if such storm-generated patterns are sufficiently large and persistent will they be retained. From this viewpoint, a goodness-of-fit measure (such as an RMS error) is not useful in determining analysis quality. Thus, only one iteration (Barnes, 1973) is performed to produce a low-pass filtered field.

2.2 Band-Pass Filter Design

A non-dimensional filter design permits application to any grid, without specifying grid length values. An appropriate characteristic length scale is the miminum resolvable wavelength, $L_\Delta = 2\Delta s$. By using this length scale, dimensional wavenumber, k*, is given a non-dimensional value, k, according to

$$k = \frac{k^*}{k_\Delta} \quad , \tag{4}$$

where k_Δ is the characteristic wavenumber,

$$k_\Delta = \frac{2\pi}{L_\Delta} \quad . \tag{5}$$

If a general wave of length L* is considered to be some number, λ, (not necessarily an integer) of grid intervals long, the wavenumber of that wave is given by

$$k = \frac{2\pi}{\lambda \Delta s} \frac{L_\Delta}{2\pi} = \frac{2}{\lambda} \quad . \tag{6}$$

A similar development can be made in the time/frequency domain, where waves are defined in terms of the characteristic period $p_\Delta = 2\Delta t$. Then the non-dimensional frequency, ν, is given by

$$\nu = \frac{2\pi}{\tau \Delta t} \frac{p_\Delta}{2\pi} = \frac{2}{\tau} \quad , \tag{7}$$

where a general wave of period p* is considered to be τ time intervals long. As (6) and (7) imply, in the non-dimensional k (or ν) system, the wavenumber varies from zero at the spatial (temporal) mean, to unity at the spatial (temporal) Nyquist wavenumber (frequency).

Consider a Barnes-type response function/weight function pair in the spatial domain:

$$\begin{aligned} r_s\ (k^*;\ \kappa) &= e^{-\kappa k^{*2}} \quad , \\ \tilde{w}_s\ (R^*;\ \kappa) &= e^{-R^{*2}/4\kappa} \quad . \end{aligned} \tag{8}$$

To within a constant, as shown by Barnes, these constitute a Hankel Transform pair. In transforming to non-dimensional variables, R* is non-dimensionalized by using the characteristic $R_\Delta = \rho \Delta S$, where ρ is an arbitrary constant. Thus, the non-dimensional radius is R, where

$$R = \frac{R^*}{\rho \Delta s} \quad . \tag{9}$$

If the analysis parameter, κ, is defined in terms of a non-dimensional number, D, such that

$$\kappa = D^2\ \Delta s^2 \quad , \tag{10}$$

then by using (9) and (10), the response function/weight function pair (8) becomes

$$r_s\ (k;\ D) = \exp\ [-(\pi Dk)^2]\ ,$$

$$\tilde{w}_s\ (R;\ D) = \exp\ [-(\rho R/2D)^2]\ . \tag{11}$$

A similar analysis in the time domain yields

$$r_t\ (\nu;\ N) = \exp\ [-(\pi N\nu)^2]\ ,$$

$$\tilde{w}_t\ (T;\ N) = \exp\ [-(\gamma T/2N)^2]\ , \tag{12}$$

where the non-dimensional time separation (γ is the temporal analogue to ρ) is T, given by

$$T = \frac{T^*}{\gamma \Delta t}\ , \tag{13}$$

and the temporal analysis parameter, η, is defined in terms of N, a non-dimensional number such that

$$\eta = N^2\ \Delta t^2\ . \tag{14}$$

To use (11) and (12) to develop a band-pass filter, define

$$\Delta r_{ij}^{(m)} = r_s\ (k_i;\ D_m) - r_s(k_j;\ D_m)\ , \tag{15}$$

which is the change in response, using parameter D_m, between the i^{th} and j^{th} wavenumbers. If k_2 is to be the wavenumber where the band-pass filter's peak response is desired (the center of the band), we must simultaneously maximize

$$\Delta r_{12}^{(a)} = r_s\ (k_i;\ D_a) - r_s(k_2;\ D_a)\ ,$$

$$\Delta r_{23}^{(b)} = r_s\ (k_2;\ D_b) - r_s(k_3;\ D_b)\ , \tag{16}$$

subject to the constraint that

$$\Delta r_{12}^{(a)} = \Delta r_{23}^{(b)}\ . \tag{17}$$

Note that $k_1 < k_2 < k_3$ and that k_1 and k_3 are not true cut-off wavenumbers, in the sense that the response attains specific values (e.g., e^{-1} times peak response) at these wavenumbers. The roles of k_1 and k_3 are explained in the following paragraphs.

Use of (16) and (17) is illustrated schematically in Fig. 1. Maximum response change is attained when

$$\frac{\partial}{\partial D_a} [\Delta r_{12}^{(a)}] = 0 \ ,$$

$$\frac{\partial}{\partial D_b} [\Delta r_{23}^{(b)}] = 0 \ . \tag{18}$$

Upon using (11) and (16) in (18), it is found that

$$D_a^2 = \frac{2 \ln \left(\frac{k_1}{k_2}\right)}{\pi^2 \left(k_1^2 - k_2^2\right)} \ , \tag{19a}$$

$$D_b^2 = \frac{2 \ln \left(\frac{k_2}{k_3}\right)}{\pi^2 \left(k_2^2 - k_3^2\right)} \ . \tag{19b}$$

The constraint (17), when combined with (11) and (16), implies that

$$k_1 = \frac{1}{\pi D_a} \left\{ -\ln \left[e^{-(\pi D_a k_2)^2} + e^{-(\pi D_b k_2)^2} - e^{-(\pi D_b k_3)^2} \right] \right\} \ . \tag{20}$$

Having chosen k_2 and some value for k_3 (for which $k_2 < k_3 < 1$), it is possible to solve (19b) for D_b and use (19a) and (20) to iterate on k_1 and D_a until the system is solved. In practice, convergence is rapid.

As seen in Figs. 2 and 3, band-pass response is normalized to unity at the center of the band. If the unnormalized response difference at k_2 is

$$\delta r_s = r_s \left(k_2; D_b\right) - r_s \left(k_2; D_a\right) \ ,$$

then the normalized response is simply

$$r_{bs} = \frac{1}{\delta r_s} \left[r_s^{(b)} - r_s^{(a)} \right] \ .$$

A completely analogous argument holds in the temporal domain.

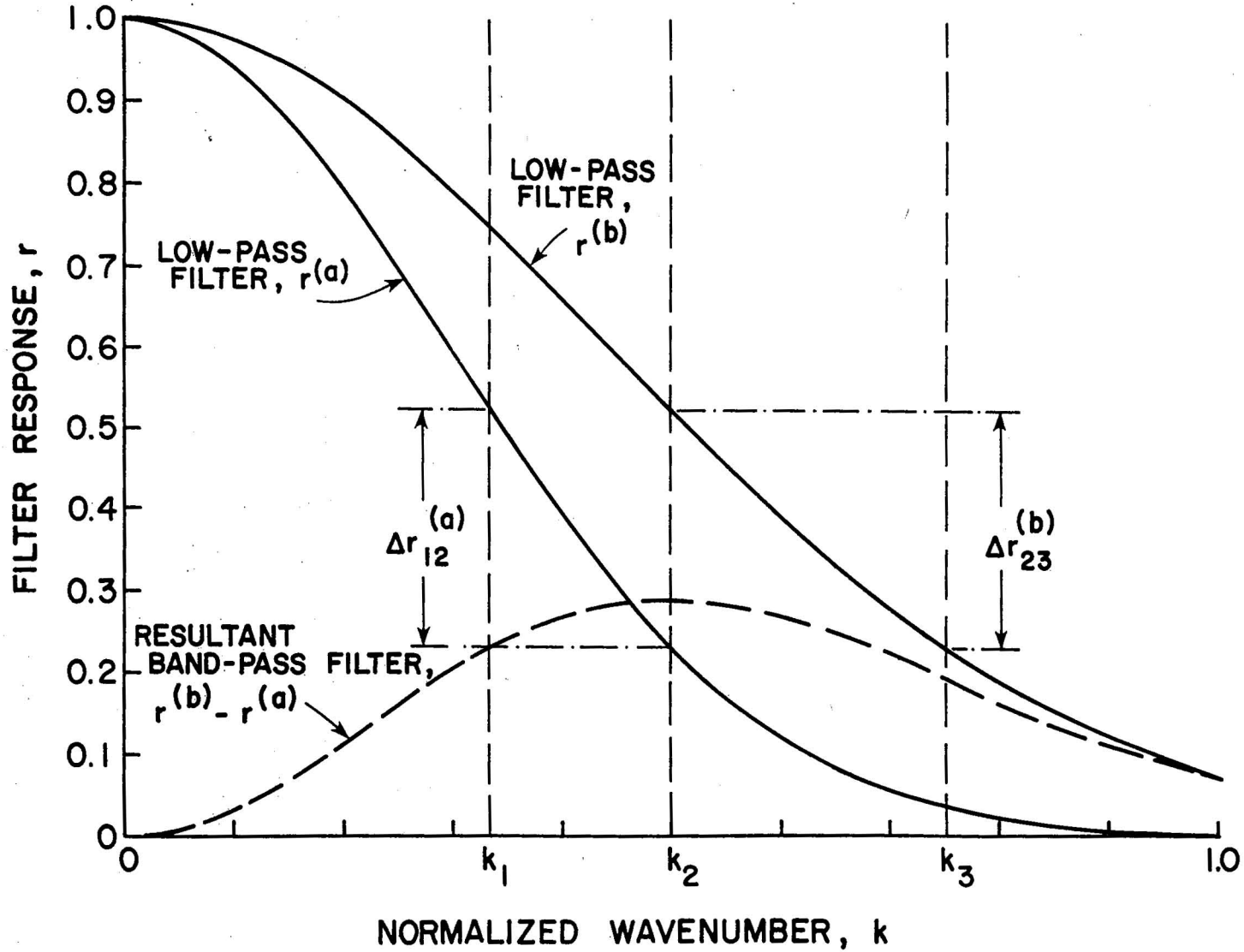

Fig. 1 *Schmatic illustration of development of band-pass filter as difference between two low-pass filters.*

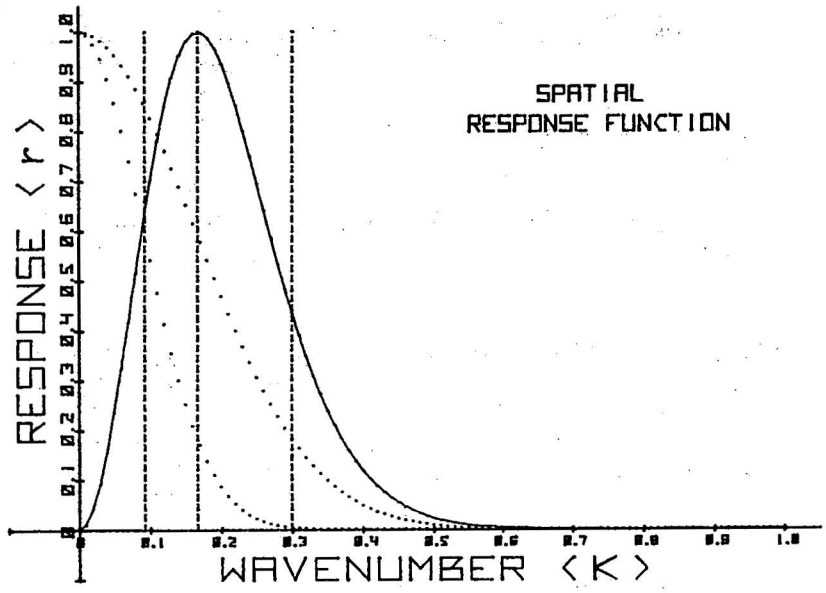

Fig. 2 Spatial response function with band-pass peak centered at 12Δs.

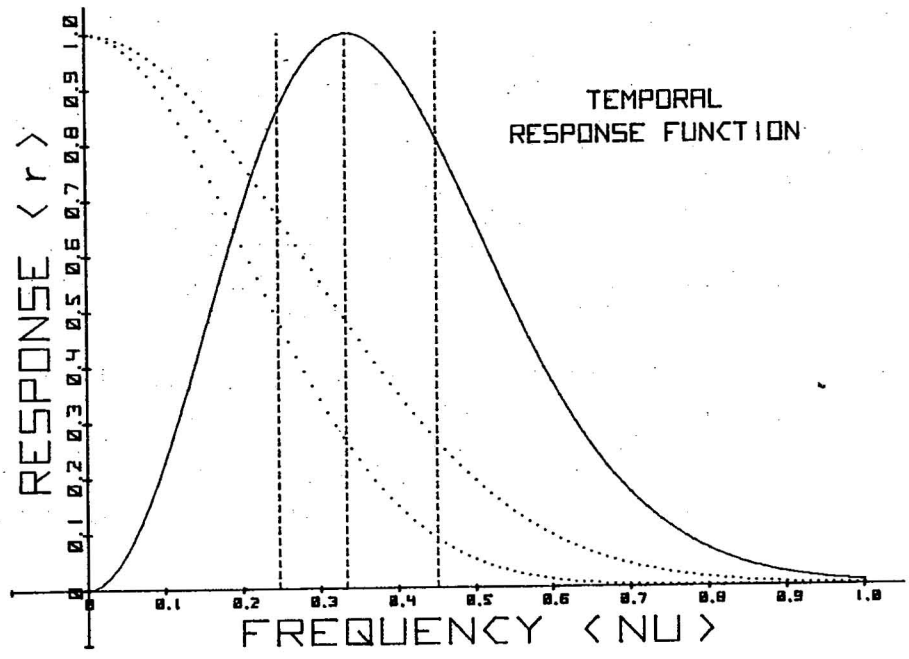

Fig. 3 Temporal response function with band-pass peak centered at 6Δt.

Band-pass filtering proceeds as follows: data are interpolated to grid points using the weight function

$$\tilde{w}_a\ (R,\ T;\ D,\ N) = \exp\ [-\ \frac{(\rho R)^2}{4D_a^2} - \frac{(\gamma T)^2}{4N_a^2}]\ ,$$

and again, using weight function

$$\tilde{w}_b\ (R,\ T;\ D,\ N) = \exp\ [-\ \frac{(\rho R)^2}{4D_b^2} - \frac{(\gamma T)^2}{4N_b^2}]\ .$$

These yield grid point values for the analyzed field of $\phi^{(a)}$ and $\phi^{(b)}$, respectively. If the bands are centered at k_2 in space and ν_2 in time, then

$$\delta r = e^{-[(\pi D_b k_2)^2 + (\pi N_b \nu_2)^2]} - e^{-[(\pi D_a k_2)^2 + (\pi N_a \nu_2)^2]}\ ,$$

and so the band-pass field is given by

$$\phi^{(b-a)} = \frac{1}{\delta r}\ [\phi^{(b)} - \phi^{(a)}]\ . \qquad (21)$$

For the purposes of this paper, a "low-pass" field is chosen to be $\phi^{(a)}$.

If the scale of the phenomenon of interest is precisely known, it is possible to center the band-pass filter at exactly that scale. In general, of course we want to look at a narrow range of scales. The aim of this research is, in part, to examine events at the resolution limits of the conventional surface data network[2]. Accordingly, it is appropriate to place the band center at or near that limit. If the center is placed at or near the Nyquist frequency (or wavenumber) for the data, then truncation error is likely to be a serious problem. There is no clear-cut lower limit for the sampling frequency to avoid truncation difficulties, but roughly six to eight samples per wave give reasonably accurate first derivative estimates.

The filter used, therefore, centers on waves that the data mesh (roughly twice the grid) samples at about six times the Nyquist interval. The response functions in space and time are shown in Figs. 2 and 3, while the corresponding weight functions are seen in Figs. 4 and 5. It may be observed that k_2 and k_3 (ν_2 and ν_3) determine a unique band-pass filter centered at k_2.

[2]That is, the subsynoptic scales of length and time fall at or near the resolution limits for that data.

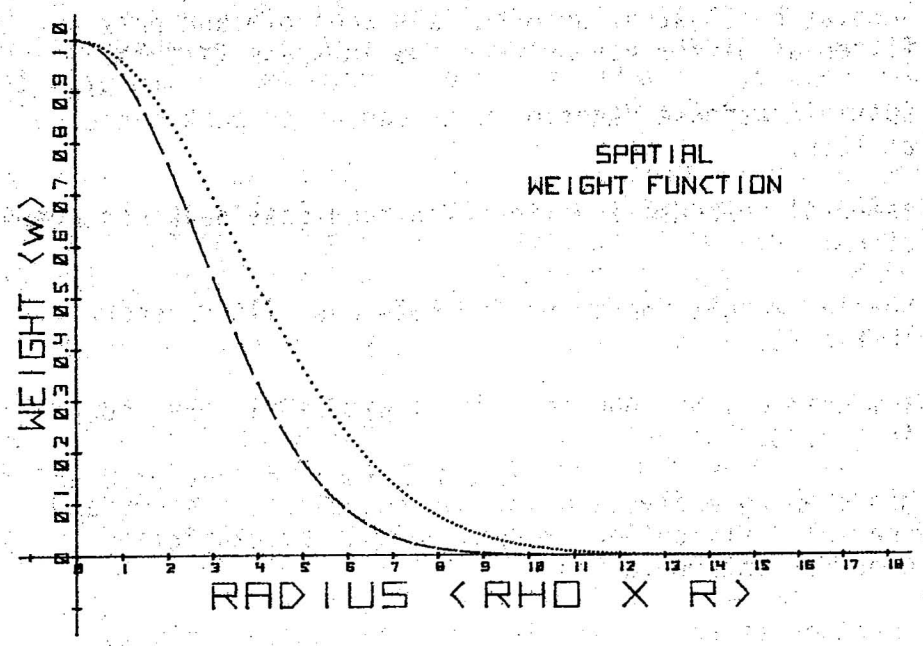

Fig. 4 Spatial weight functions for low-pass filters shown in Fig. 2.

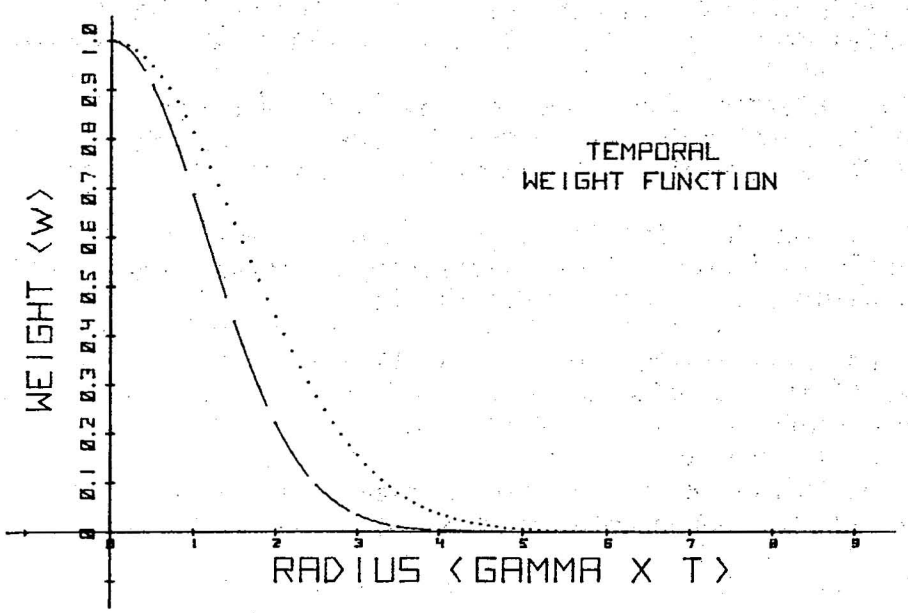

Fig. 5 Temporal weight function for low-pass filters shown in Fig. 3.

2.3 The Data and the Analysis Grid

Surface observations obtained from the original WBAN-10 (or equivalent) forms are used for this study, including all "special" and "local" observations which are frequently not transmitted. All data between 0515 and 1845 CST (including wind speed, wind direction, time of the observation, altimeter setting, temperature, and dewpoint) are transferred to magnetic tape, after being subjected to pre-filtering.

The pre-filtering removes gross errors (such as those introduced by keypunch mistakes) and obviously unrepresentative observations. An observation is considered unrepresentative when its second time derivative exceeds a threshold value selected to reject only about 40 or fewer observations out of about 1800 per data set. A rejected observation is replaced by a smoothed value obtained from a cubic polynomial fit of surrounding good data points.

Altimeter setting is used in place of the so-called sea-level pressure (SLP) for two basic reasons: first, more stations record altimeter setting more frequently; and second, the method by which altimeter setting has been reduced to sea level is the same at all stations, independent of the temperature history. This procedure introduces a diurnal trend but SLP also contains some residual diurnal trend and, additionally, such influences may be physically meaningful to severe weather activity.

The wind speed used, in the event of gusts, is the arithmetic mean of the "sustained" wind and the gust, rounded to the next highest knot, if necessary. It is felt that both extremes are unrepresentative of advective wind speeds.

Cases have been chosen by several criteria. First, the author resided in Oklahoma from 1972 to 1976 and is generally familiar with weather events during that period. Second, severe thunderstorms had to have occurred; an exhaustive test of the technique must include a variety of cases so that storm and non-storm magnitudes for the variables can be compared, but a technique has to function properly during storm events before being considered for general use. The following days were chosen: May 24, 1968; April 19, 1972; May 22, 1972; June 27, 1972; March 13, 1973; May 24, 1973; June 8, 1974; and June 18, 1973. These cases were chosen to represent several types of severe weather systems. The last case is the primary testbed for the analysis.

Interpolation is accomplished on a 25 by 19 grid, superimposed on a polar stereographic map (true at 60° N latitude with a map scale factor of $1:10^7$). The map coordinates, the grid, and the stations used in the analysis are shown in Fig. 6. The 0.25 inch grid spacing corresponds to 63.5 km. Maps of analyzed quantities are produced at hourly intervals from 0600 CST to 1800 CST. About 125 stations are used in the analysis, including those within roughly two grid lengths of the grid borders. Not all stations report hourly, especially in the western part of the grid. A terrain analysis based on the low-pass filtered station heights is shown in Fig. 7. Map coordinates shown are based on map inches from the north pole and 100° W longitude for the y and x directions, respectively.

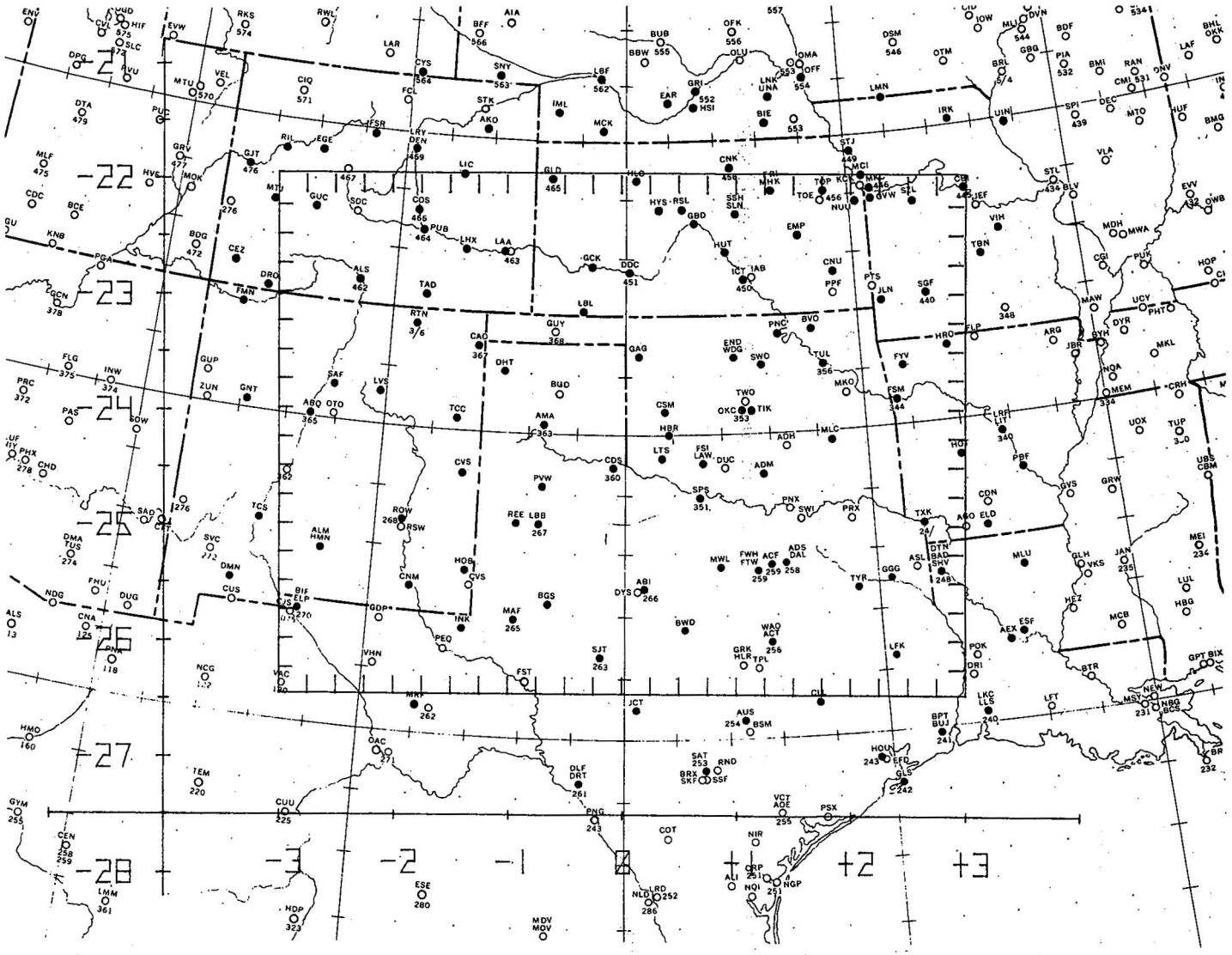

Fig. 6 *Map showing analysis grid, map coordinate system, and spatial distribution of data points (black circles) used for interpolation.*

Fig. 7 Smoothed terrain analysis based on station heights, in meters.

3. RESULTS OF FILTERING - JUNE 18, 1973

The band-pass filter is applied to surface data for this case (also studied by Siebers et al. 1975) which involves relatively isolated severe weather events. Upper air data at 0600 CST indicate a strong trough in the western United States extending southward from a low center located in Montana. There are two minor short waves imbedded in this trough--one extending into western Kansas and another into central Arizona. The 500 mb winds in the base of the trough are about 10 m s^{-1} from Arizona to Illinois. Isotherms at 500 mb show no indication of cold air advection that might affect Oklahoma. At 700 mb, a weak thermal ridge lies along a line from the Big Bend area in Texas, through the Texas and Oklahoma Panhandles into west central Kansas, with moderate cold air advection in the base of the major trough. A broad band of moisture at 850 mb extends from southern Texas through Oklahoma and extreme eastern Kansas into Iowa, ahead of a well-defined trough axis. A wedge of dry, warm air separates this moist air from a strong 850 mb cold front in central Kansas through the extreme western Oklahoma Panhandle into northern New Mexico. Winds at 850 mb in the moist air are southwesterly at speeds of 15 to 25 m s^{-1}, and are northwesterly at about 25 m s^{-1} in the cold air to the north.

To summarize the synoptic pattern for this case, the upper-air pattern is relatively weak, with an apparent strengthening of the system as one approaches the surface. Moist air ahead of the front is quite unstable, and many of the 700 mb and 850 mb parameters mentioned by Miller (1972) as favorable for severe weather, are moderate to strong, while the 500 mb parameters are weak. This situation is not typical of a classic severe weather outbreak, but it does represent many severe weather situations during late spring, when the polar jet stream is usually well north of Oklahoma.

As seen in the figures presented, spatial continuity of the analyzed fields seems satisfactory. To examine the temporal continuity of filtered surface data, assume that the "u-component" of the wind field (basically, the eastward component, on this analysis grid) is the field most likely to exhibit excessively rapid temporal variation. This is a reasonable assumption, especially since wind components are the noisiest data with which we deal. By showing satisfactorily continuous results for the u-component, we can infer that the rest of the analyzed fields show good time continuity. Fig. 8 shows the hourly values of the u-component at a centrally located grid point; the temporal behavior is, indeed, quite smooth. An examination of the time evolution of the spatial patterns (not shown) confirms this conclusion.

Consider the low-pass results seen in Fig. 9 at 1200 CST. The streamline/isotach pattern reveals the dominant frontal convergence zone across Oklahoma from southwest to northeast. This convergence zone is associated, but not coincident, with a pressure trough and is characterized by cyclonic relative vorticity. The mixing ratio field shows a distinctive pattern, curving southward in western Oklahoma where the surface dryline intersects the surface cold front. The axis of maximum moisture convergence is approximately coincident with the dryline, while kinematic convergence lags somewhat behind the dryline, in agreement with the findings of Schaefer (1974) for quiescent dryline situations. The dryline is not clearly depicted in the low-pass streamline field, but it shows clearly as the trailing edge of a band of high

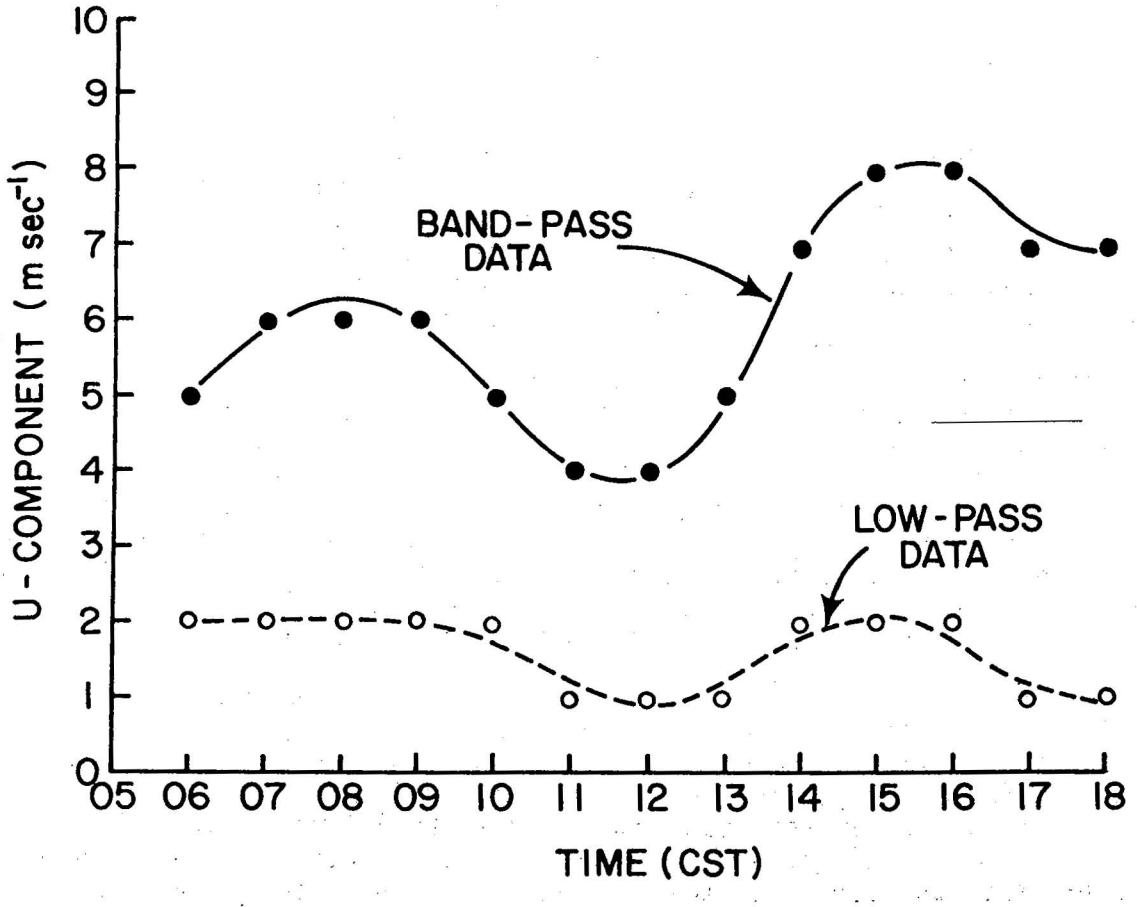

Fig. 8 Hourly values of u-component (to the nearest m s^{-1}) for low-pass data (open circles) and band-pass data (dark circles). The curves shown an approximate continuous interpolation.

isobaric crossing angles that extends southward from central Oklahoma. Wind speeds are basically subgeostrophic everywhere (as might well be anticipated at the surface) with ageostrophic speed maxima associated with low crossing angles in the moist air and high crossing angles in the dry air. An ageostrophic speed minimum lies in the pressure trough. Crossing angles are relatively low in both the cold and the moist airmasses.

With only minor changes, these low-pass patterns remain nearly fixed throughout the 12-hour analysis period. This is, in part, a result of the filtering. Nevertheless, the remarkable consistency of the crossing angle pattern suggests that this large scale flow is being influenced by a systematic, relatively time-independent process which causes a characteristic departure from geostrophic balance. The pattern is not suggestive of frictional effects, as it is neither strongly dependent on terrain nor on time of day. This subject is examined further in a later section.

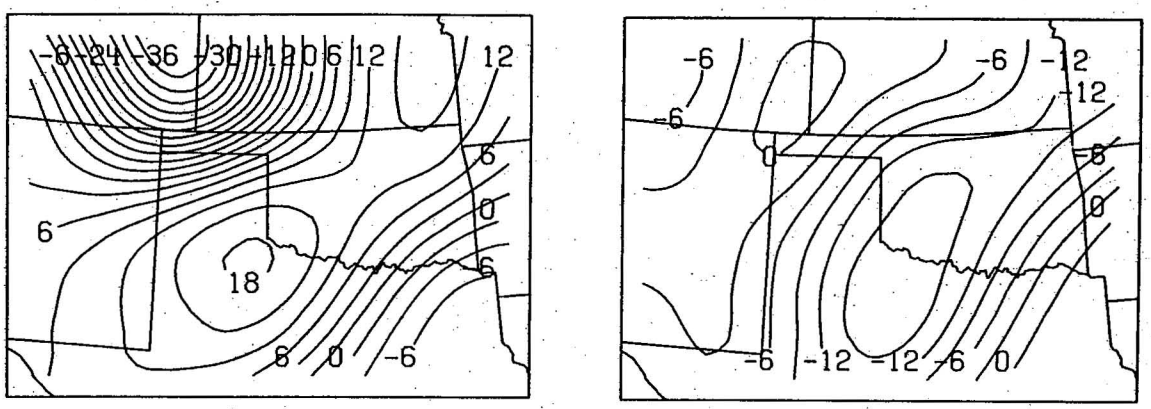

LOW-PASS VORTICITY

LOW-PASS DIVERGENCE

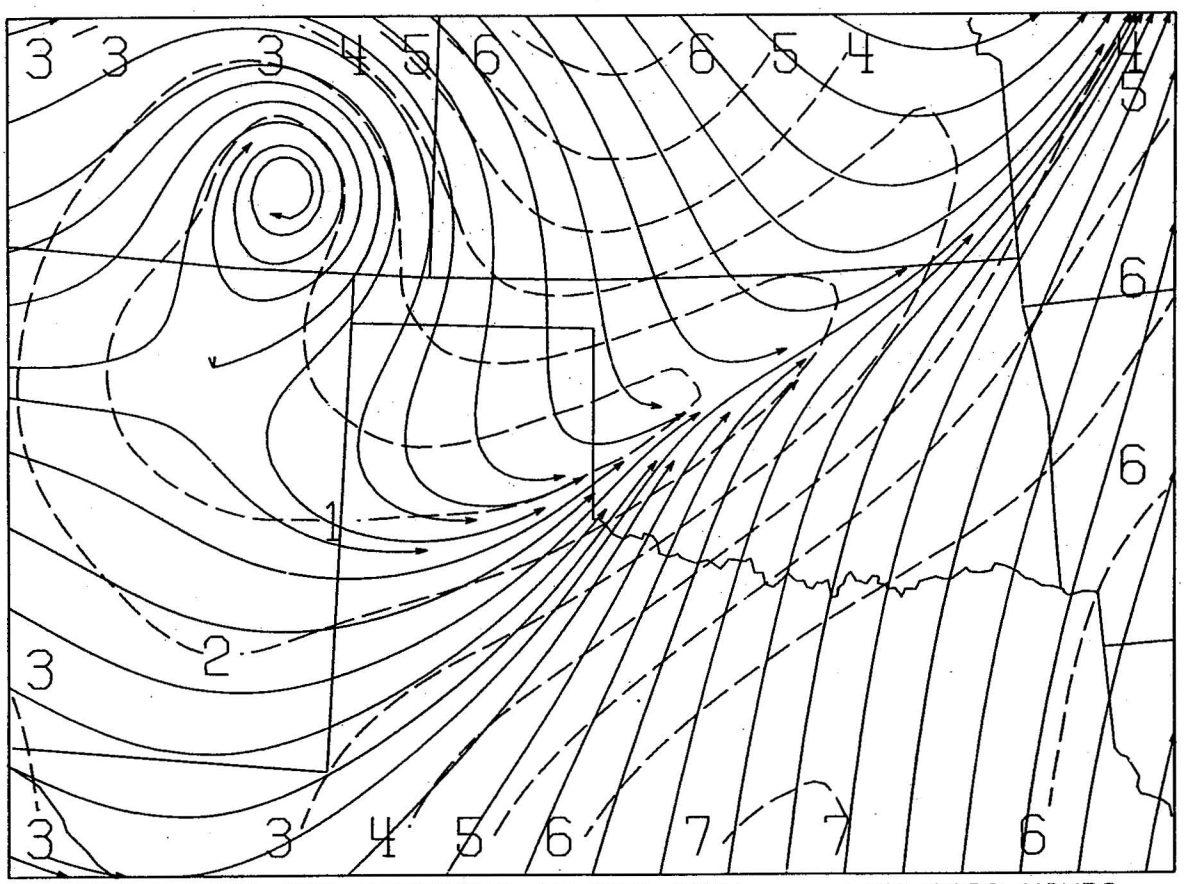

STREAMLINES AND ISOTACHS (M PER SEC) -- LOW-PASS WINDS

Fig. 9a Low-pass results for June 18, 1973 at 1200 CST. Vorticity and divergence are multiplied by 10^6 and units are sec^{-1}.

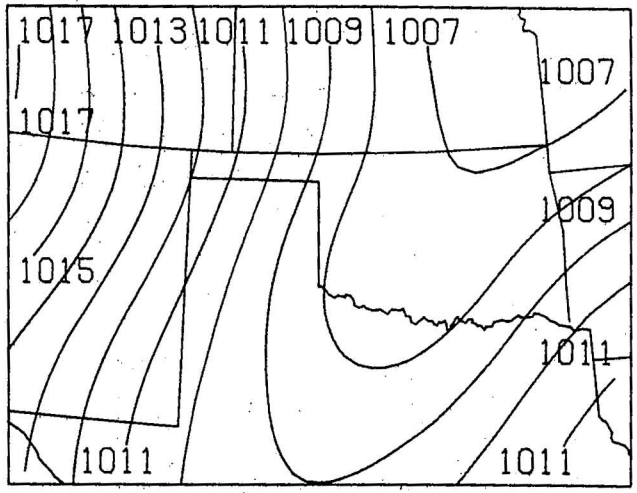

LOW-PASS ALTIMETER SETTING

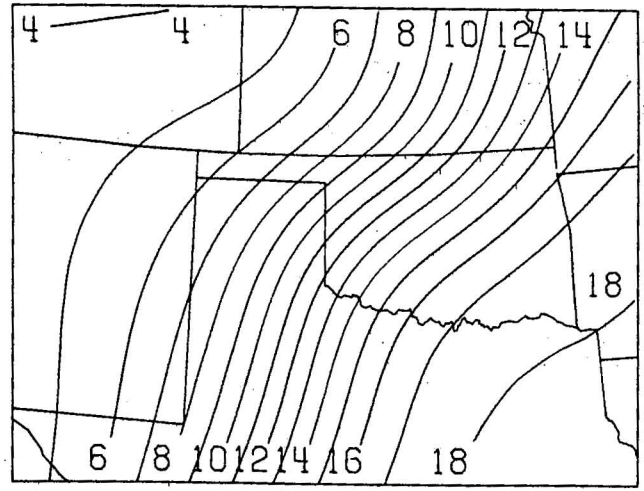

LOW-PASS MIXING RATIO

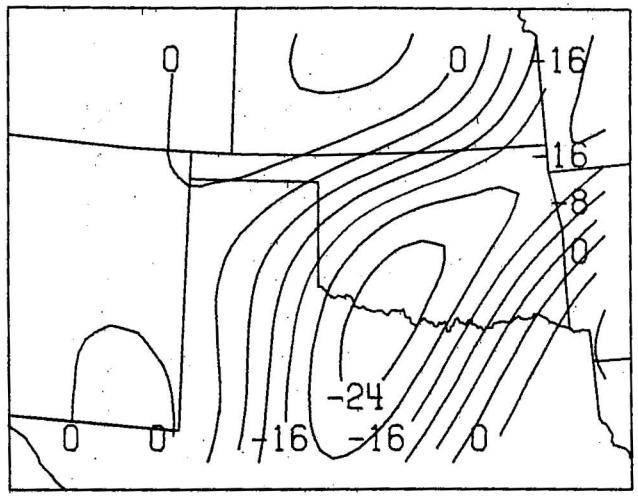

LOW-PASS MOISTURE DIVERGENCE

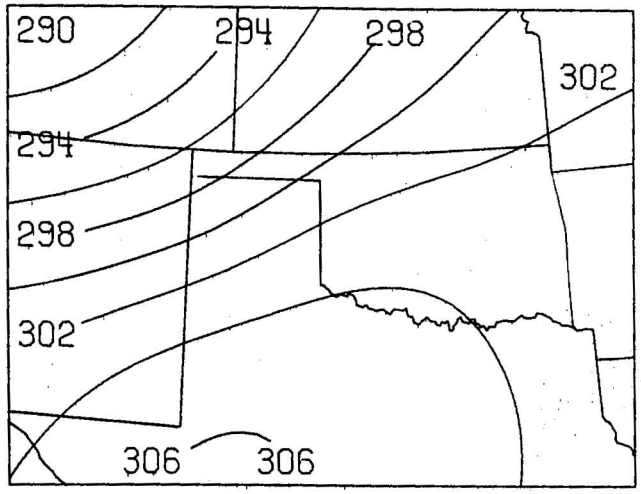

LOW-PASS TEMPERATURE

Fig. 9b *Altimeter setting in mb, mixing ratio in g kg^{-1}, moisture divergence is multipled by 10^5 and has units of g kg^{-1} sec^{-1}, temperature in deg k.*

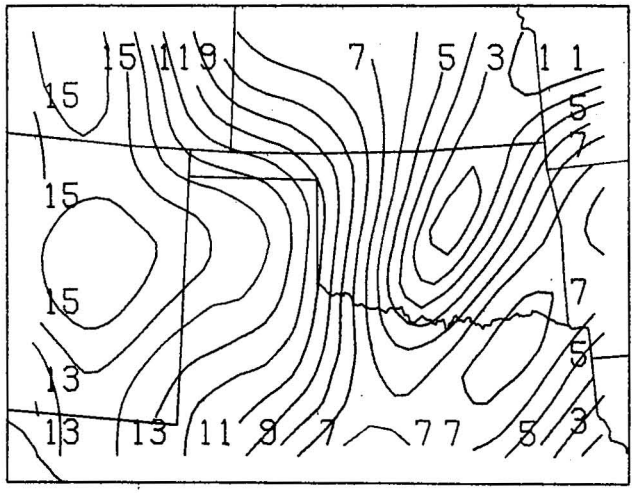

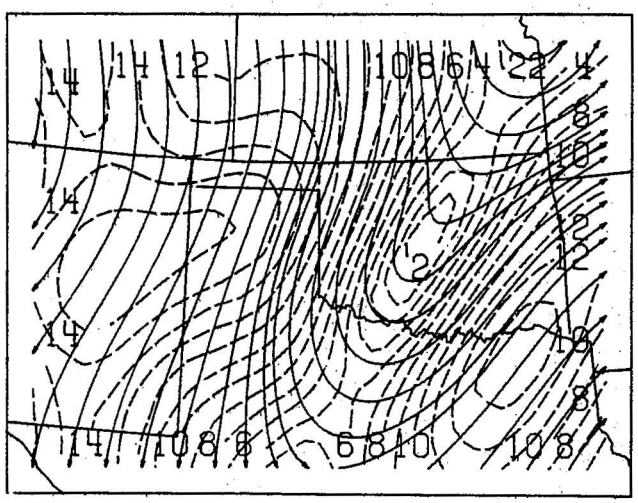

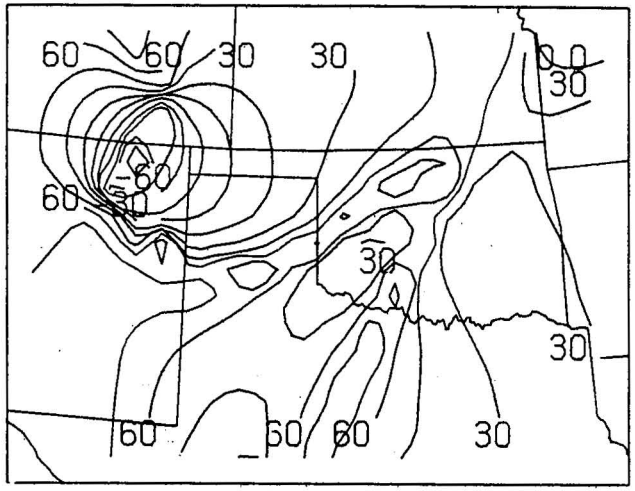

Fig. 9c *Ageostrophic speed in m sec^{-1}, isobaric crossing angle in degrees with positive angles toward low pressure, geostrophic isotachs in m sec^{-1}.*

Band-pass fields (Fig. 10) naturally reveal smaller scale temporal and spatial features. The most striking feature in the streamline/isotach field at 1200 CST is the cyclonic circulation in southwest Oklahoma. The associated frontal zone and dryline are seen in greater detail and this cyclone is associated with the dryline/front intersection. The center of circulation has moved out of the central Texas Panhandle area since 0600 CST and is now (at 1200 CST) almost coincident with the nearly stationary band-pass pressure minimum. There are several noteworthy features in the derived properties of this flow field. Significant cyclonic vorticity extends westward from the circulation center, which is interpreted as the westward extension of the cold front. The large kinematic convergence maximum (still behind the dryline) south of the circulation has developed rapidly since 0900 CST, coincident with an increase in the westerly component in the dry air. This was accompanied by a rapid temperature rise and a sharp moisture decrease. The three moisture convergence maxima apparent at 1200 CST have evolved separately: the first, northeast of the circulation, as a feature in slow decline (since 0600 CST); the second caused by the rapid increase in kinematic convergence near the dryline just discussed; and the third being a separate, persistent frontal feature in extreme northeastern Oklahoma.

The satellite photo (Fig. 11) at about the same time, reveals only a band of towering cumulus along the front which apparently terminates near the center of circulation. However, the picture taken several hours later (Fig. 12) shows active severe thunderstorms which coincide remarkable well with the three moisture convergence centers. The storms' time history indicates that severe weather occurs only after several hours of substantial pre-existing (band-pass) moisture convergence. Activity in Texas, south of the Red River in the convergence zone associated with the dryline, is only beginning to develop by 1642 CST, whereas storms in Oklahoma are already producing tornadoes.

The success of band-pass moisture convergence in delineating preferred areas of storm development several hours before storm initiation is, perhaps, the technique's most convincing demonstration. Although this case is exceptionally well-defined, most other cases studied seem to fit this general pattern. Some of the cases suggest the dominance of scales of motion above or below the scale chosen here. Among the eight cases studied so far, four were of the sort depicted in this section. Two cases were clearly synoptic in character and two appeared to be below the resolution limits for surface data. Thus, on any given severe weather day the organizing dynamics may be predominately synoptic or, perhaps, well below the limits of surface data resolution. However, a substantial amount of severe weather that occurs in the southern Great Plains is characterized by organizing dynamics that seem to fall in the subsynoptic range emphasized with this band-pass filter.

4. SCALE ANALYSIS OF SUBSYNOPTIC SYSTEMS

Despite the scarcity of definitive upper air observations on the subsynoptic scale, we can proceed with a formal scale analysis, using surface data when available. Estimates for the vertical variations can be derived ir part from numerical simulations and in part from inference from the surface data. The scaling follows the procedures outlined in Haltiner (1971).

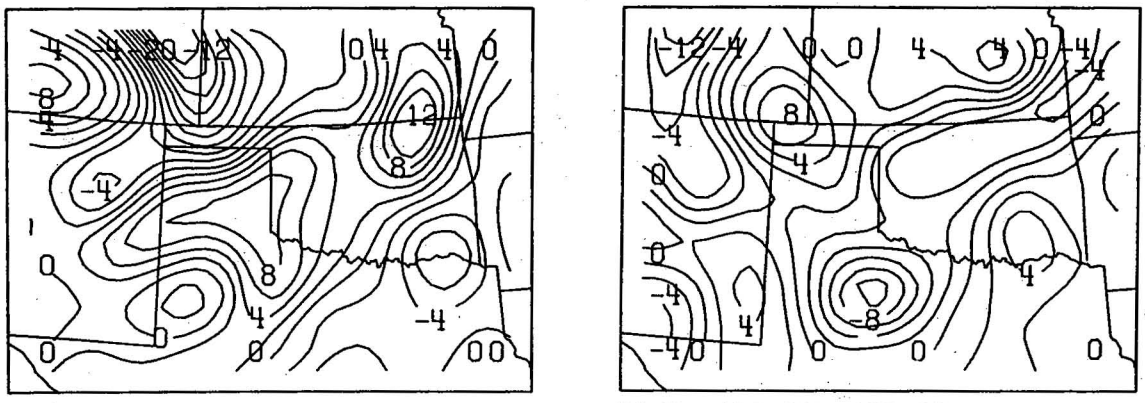

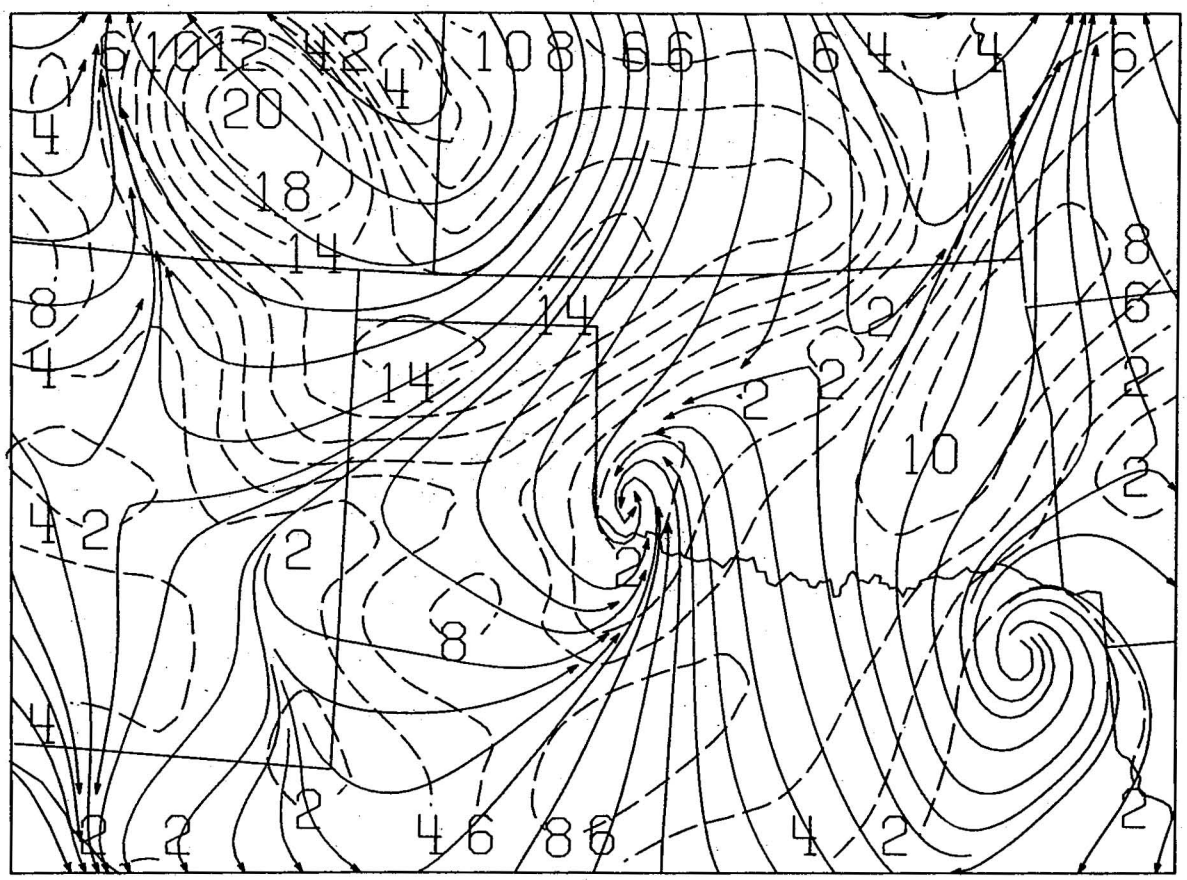

Fig. 10a Band-pass results for June 18, 1973 at 1200 CST. Vorticity and divergence are multiplied by 10^5 and units are sec^{-1}.

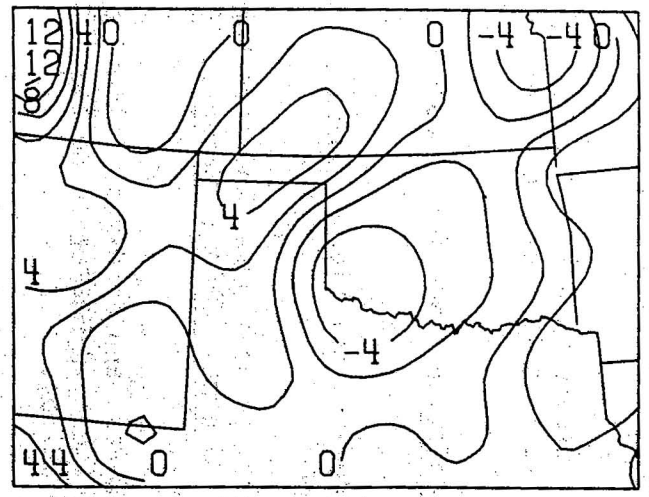

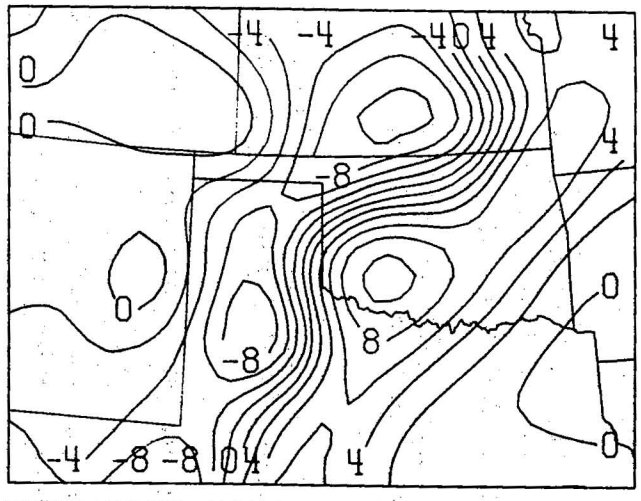

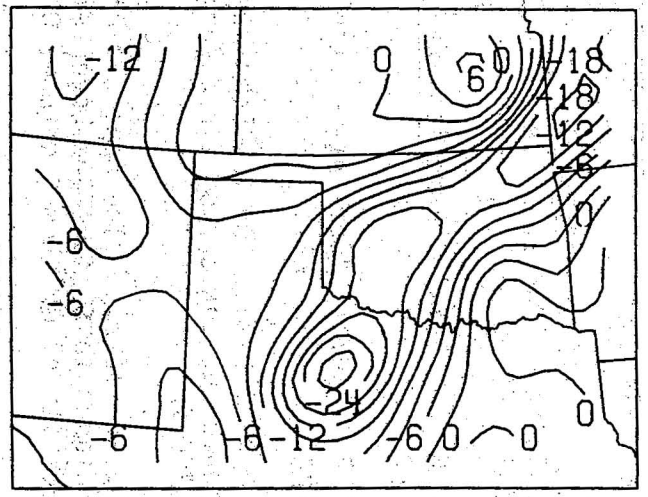

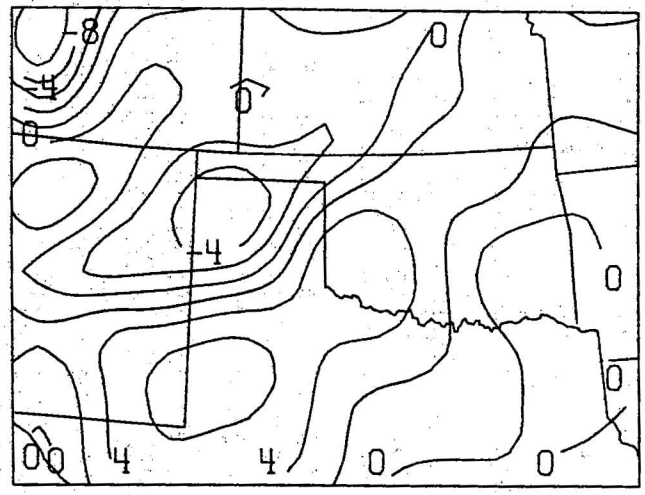

Fig. 10b *Same as Fig. 8, except for band-pass results and moisture divergence is multiplied by* 10^4.

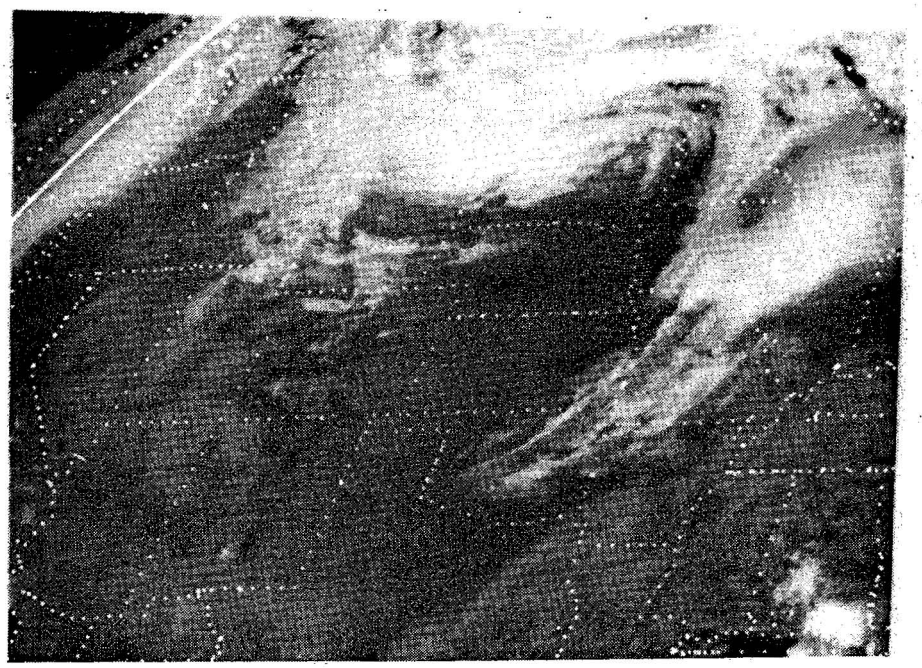

Fig. 11 *Satellite photo at 1221 CST on June 18, 1973.*

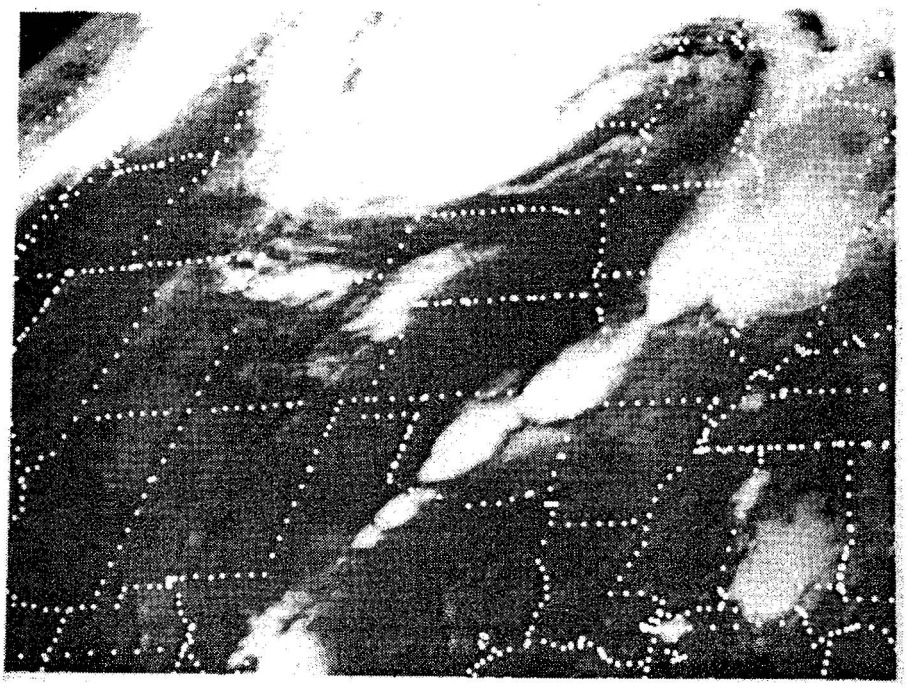

Fig. 12 *Satellite photo at 1642 CST on June 18, 1973.*

In specifying characteristic values, a more specific definition of the term "subsynoptic" is provided. Physical scales in space and time are:

L....Characteristic horizontal scale (about a quarter wavelength);

D....Characteristic depth scale (also a quarter wavelength);

H....Scale height of the atmosphere;

V,W..Characteristic horizontal and vertical velocity amplitudes;

τ....Characteristic period (advective period).

The notation here follows Haltiner; however, characteristic values reflect the difference in scales. Here we use

$$V = 20 \text{ m s}^{-1},\ L = 2 \times 10^5 \text{m},\ D = 2.5 \times 10^3 \text{m} ,$$

which implies $\tau = 10^4$ s. The magnitude of W is to be developed.

This analysis is concerned only with medium scale flow and does not include the synoptic scale terms and their interactions on this scale. Specifically, if we suppose that any general physical variable ϕ is the sum of three basic components--i.e., a large scale, a medium scale, and a small scale---so that

$$\phi = \phi_L + \phi_M + \phi_S ,$$

then ϕ_M is associated with the band-pass results, i.e.,

$$\phi^{(b)} - \phi^{(a)} = \phi_M ,$$

where the superscripts a and b, as in the preceding chapter, denote the values produced by low-pass filters with different response. Linear terms like

$$\frac{\partial \phi_M}{\partial t} = \frac{\partial \phi^{(b)}}{\partial t} - \frac{\partial \phi^{(a)}}{\partial t} ,$$

present no difficulty in scale separation. However, nonlinear terms are more troublesome. For example, consider

$$u \frac{\partial \phi}{\partial x} = (u_L + u_M + u_S) \frac{\partial}{\partial x} (\phi_L + \phi_M + \phi_S) .$$

When the products are low-pass filtered, the results are

$$(u\frac{\partial\phi}{\partial x})(b) = (u_L + u_M)\frac{\partial}{\partial x}(\phi_L + \phi_M) ,$$

and

$$(u\frac{\partial\phi}{\partial x})(a) = u_L\frac{\partial\phi_L}{\partial x} ,$$

so that the difference of the products is given by

$$(u\frac{\partial\phi}{\partial x})(b) - (u\frac{\partial\phi}{\partial x})(a) = u_M\frac{\partial\phi_L}{\partial x} + u_L\frac{\partial\phi_M}{\partial x} + u_M\frac{\partial\phi_M}{\partial x} .$$

However, the product of the differences is simply

$$(u^{(b)} - u^{(a)})\frac{\partial}{\partial x}(\phi^{(b)} - \phi^{(a)}) = u_M\frac{\partial\phi_M}{\partial x} .$$

Characteristic values of u and ϕ may be different between the scales--e.g., if ϕ is temperature, assume that

$$V_L \sim 10 \text{ m s}^{-1},\ V_M \sim 20 \text{ m s}^{-1},\ L_L \sim 10^6 \text{ m} ,$$

$$\phi_L \sim \Phi \text{ °K},\ \phi_M \sim 2\Phi \text{ °K},\ L_M \sim 2 \times 10^5 \text{ m} ,$$

so that

$$u_M\frac{\partial\phi_L}{\partial x} \sim \frac{V_M\Phi}{L_L} \sim 2\Phi \times 10^5 \text{ °K s}^{-1} ,$$

$$u_L\frac{\partial\phi_M}{\partial x} \sim \frac{2V_L\Phi}{L_M} \sim \Phi \times 10^4 \text{ °K s}^{-1} ,$$

$$u_M\frac{\partial\phi_M}{\partial x} \sim \frac{4V_M}{L_M} \sim 2\Phi \times 10^{-4} \text{ °K s}^{-1} .$$

In the scale analyses to follow, only the term $u_M\frac{\partial\phi_M}{\partial x}$ is considered, which ignores any interaction terms, as they are likely to be of the same order as the terms we include (or, perhaps, of lower order). This is not to imply that interaction terms are not significant. Such effects are not considered in this study.

The Rossby number, Ro, is defined as

$$Ro = \frac{V}{f_o L} \quad , \tag{22}$$

where f_o is the characteristic value of the Coriolis parameter ($f_o \sim 10^{-4} s^{-1}$). By the above, Ro ~ 1. Furthermore, we assert that the Richardson number, Ri, defined by

$$Ri = \frac{g \frac{\partial (\ln \theta)}{\partial z}}{\left(\frac{\partial V}{\partial z}\right)^2} \quad ,$$

is also of order unity. This assertion is examined in a later discussion. Finally, the Froude number, Fr, given by

$$Fr = \frac{V^2}{gD} \quad , \tag{23}$$

is of order 10^{-2}.

Using Haltiner's (3.23), along with (22) and (23), and Haltiner's (3.21), which shows that

$$\frac{\partial \ln \theta_s}{\partial z} \sim \frac{\sigma_s}{D} \quad ,$$

where σ_s is the stability parameter of the standard atmosphere ($\sigma_s \sim 10^{-1}$), it is found that

$$W \sim \frac{D}{RiRo} \frac{V}{L} \quad . \tag{24}$$

This gives $W \sim 2.5 \times 10^{-1}$ m s^{-1} (about 25 cm s^{-1}). This value is about three times larger than the numerical simulations of Tokioka (1972) or Nitta and Ogura (1972). Following Haltiner, the order of the pressure terms is

$$\delta p' \sim \frac{DFr}{HRo} \sim 4 \times 10^{-3} \quad , \tag{25}$$

where $H \sim 10^4$ m. This implies a dimensional pressure perturbation of about 8 mb, which is also in rough agreement with numerical simulations.

The vector horizontal equation of motion is

$$\frac{\partial \vec{V}}{\partial t} + \vec{V} \cdot \nabla \vec{V} + w \frac{\partial \vec{V}}{\partial z} = - \alpha \nabla p + f \hat{k} \times \vec{V} + \vec{F} \quad , \tag{26}$$

where $\vec{F}$ is the friction term. If we follow Lewis (1971) and replace this term by $\kappa\vec{V}$, and use a value for $\kappa = 8 \times 10^{-5} s^{-1}$ (Haurwitz, 1947), then all terms in this equation are of order 10^{-3} m s^{-2}. This suggests that, based on preliminary estimates, no dynamic balances exist for subsynoptic scale motions.

As shown in numerous texts, including Haltiner's, if the characteristic depth is sufficiently small compared to the characteristic length, the hydrostatic assumption is justified. In this case,

$$\frac{D^2}{L^2} \sim 10^{-4} << 1 \quad ,$$

so we can legitimately assume hydrostatic equilibrium.

For the conservation of energy (First Law of Thermodynamics), we again call on Haltiner's analysis. In his notation (Page 52), using (24)

$$\left(\frac{\partial}{\partial t} + \vec{V} \cdot \nabla\right) \ln \theta \sim \frac{V}{L} \frac{Fr}{Ro} \sim 10^{-6} \quad ,$$

$$w \frac{\partial \ln \theta_s}{\partial z} \sim \frac{V}{RiRo} \frac{\sigma_s}{L} \sim 10^{-5} \quad ,$$

$$w \frac{\partial}{\partial z} \left(\frac{\delta\theta'}{\theta_s'}\right) \sim \frac{V}{L} \frac{Fr}{Ro} \sim 10^{-6} \quad , \tag{27}$$

where $\delta\theta'/\theta_s'$ is the ratio of the non-dimensional perturbation of θ to the non-dimensional characteristic value of θ (see Haltiner, Page 47). These results indicate that the isentropic assumption on this scale is questionable, since the second term is not balanced by either of the others. Thus, the anisentropic form is required, which is

$$\left(\frac{\partial}{\partial t} + \vec{V} \cdot \nabla + w\frac{\partial}{\partial z}\right) \ln \theta = \frac{Q}{c_p T} \quad , \tag{28}$$

where W is the anisentropic heating rate. That anisentropic effects play a significant role has been suggested by Gall (1976a,b) and Nitta and Ogura (1972).

In the preceding, an implicit assumption is that the mass continuity equation can be scaled so that

$$\frac{V}{L} \sim \frac{W}{D} \quad . \tag{29}$$

This is not the case for all scales, as shown in all standard texts, but (24) implies that since both Ri, Ro ~ 1, (29) is valid. This also indicates that

on this scale the vorticity and divergence are of the same order. The relatively shallow nature of this type of disturbance allows the neglect of vertical density variation effects in the mass continuity equation (for scaling purposes).

Consider the assumption that Ri ~ 1. When deriving (24), the order of the static stability term was established through

$$\frac{\partial \ln \theta}{\partial z} \sim \frac{\sigma_s}{D} \quad .$$

The value of 10^{-1} for σ_s has been established for the standard atmosphere, using the total depth of the troposphere to estimate $\delta\theta/\theta$. If the value of $\delta\theta/\theta$ is chosen to be appropriate for a layer of depth D, in contact with the surface, then one might use

$$\frac{\delta\theta}{\theta} \sim \frac{Fr}{Ro} \quad ,$$

which, in our case, is of order Fr, since Ro ~ 1. Thus,

$$Ri \sim \frac{\frac{g}{D}\frac{\delta\theta}{\theta}}{\frac{V^2}{D}} = \frac{gD}{V^2} Fr \sim 1 \quad .$$

There is an element of inconsistency in this argument, which can be justified only in part by the following discussion.

Studies by McGinley (1973) and Sasaki (1973) show that Ri takes on a range of values from 10^{-1} to 10 in the areas wherein subsynoptic circulations develop. It is not entirely clear that one can establish a single value of Ri that applies to a region within which the vertical stratification varies significantly. Also, the findings of Schaefer (1976) show that, by varying the depth of the layer over which $\delta\theta/\theta$ is estimated, substantially different values can result, even in horizontally homogeneous regions. If we assume that the issue of a characteristic value for Ri is not completely established from this scale analysis, the results of analysis of real data may help to resolve the problem. Note that the analysis and computation of Gambo (1970a, b) stress that Ri ~ 1 if the medium (subsynoptic) scale divergence is to be of comparable order to the vorticity and that

$$\nabla \cdot \vec{V} \sim \frac{\zeta}{RiRo} \quad .$$

This issue is to be examined when discussing the dynamics on this scale.

Finally, consider the anisentropic heating mentioned earlier. The dry air west of the surface dryline in Great Plains subsynoptic systems is characterized by steep lapse rates over a deep layer (Schaefer, 1973; McFarland, 1975).

It is reasonable to propose that a substantial anisentropic effect could be realized by turbulent mixing in such an airmass. Neglecting the two smallest terms in the anisentropic statement of the First Law:

$$w \frac{\partial \ln \theta_s}{\partial z} = \frac{Q}{c_p T} = \frac{d \ln \theta}{dt} \quad , \tag{30}$$

where (27) requires that Q be approximately 3 joule kg^{-1} s^{-1}. Assuming that this is the result of turbulent heat flux divergence, then

$$\frac{Q}{c_p T} = \frac{\partial \tilde{H}}{\partial z} \quad , \tag{31}$$

where $\tilde{H} \sim \overline{w'\theta'}$, the turbulent heat flux. Now the turbulent heat flux can be modeled via an eddy coefficient approach, i.e.,

$$\tilde{H} = K_H \frac{\partial \ln \theta}{\partial z} \quad . \tag{32}$$

As before, there is some ambiguity in estimating the lapse rate of $\ln \theta$. If (32) is used in (31) and (30), it is clear that

$$w \frac{\partial \ln \theta_s}{\partial z} \sim \frac{\partial}{\partial z} \left(K_H \frac{\partial \ln \theta}{\partial z} \right) . \tag{33}$$

In estimating $\partial \ln \theta / \partial z$, if it is assumed that the lapse rate terms on both sides of (33) are of the same order (σ_s / D), then

$$K_H \sim WD \sim 5 \times 10^2 \quad . \tag{34}$$

If, instead, on the right-hand side of (33), $\partial \ln \theta / \partial z$ is of order Fr/D, (34) is changed to

$$K_H \sim WD \frac{\sigma_s}{Fr} \sim 5 \times 10^3 \quad . \tag{35}$$

The value of 5×10^2 $m^2 s^{-1}$ seems more reasonable, from the results of McGinley (1973) and by direct calculations in a higher order closure model (Burk, personal communication). Also, the estimates of Wu (1965) suggest that while (35) may be representative over very shallow layers, (34) seems more appropriate for this study.

In the moist air ahead of the dryline, where severe convection is expected, latent heat release could account for the anisentropic effect. Suppose

C is the condensation rate and L is the latent heat of condensation ($L \sim 2.4 \times 10^6$ joule kg^{-1}). Then the anisentropic heating rate per unit mass from condensation is simply

$$Q = LC \ . \tag{36}$$

Now, by the scale analysis $Q/c_pT \sim 10^{-5}\ s^{-1}$ with $c_pT \sim 3 \times 10^5$ joule kg^{-1}, so (30) implies

$$C \sim 1.25 \times 10^{-6}\ s^{-1} \ ,$$

or, in conventional units

$$C \sim 1.25 \times 10^{-3}\ g\ kg^{-1}\ s^{-1} \ ,$$

which is the same order as the band-pass moisture convergence we have computed for the subsynoptic scale--i.e.,

$$\nabla\cdot(rV) \sim \frac{V}{L}\, r \sim 10^{-3}\ g\ kg^{-1} s^{-1} \ ,$$

if $r \sim 10\ g\ kg^{-1}$. Hence, there is substantial agreement with the results of Fritsch (1975) who points out that severe convection cycles both total mass and water mass substantially faster (by an order of magnitude) than can be resupplied by large scale convergence. Our results suggest that subsynoptic moisture convergence is adequate to account for the water mass budget of severe convection, and that the latent heat released in the convection process can account for the anisentropic heating in the moist air.

5. SUBSYNOPTIC SCALE DYNAMICS

As suggested in the Introduction, there is a modest amount of dynamical theory available in the literature on this scale. No general agreement exists about the primary mechanisms responsible for severe weather situations. Substantial numbers of tornadoes and severe thunderstorms develop in association with what could be called "synoptic" scale weather systems (e.g., June 8, 1974). The severe weather events in such a situation are widespread and, as Ostby (1975) suggests, are relatively well treated by conventional forecast methods. Other situations (such as the June 18, 1973 event) are characterized by somewhat isolated clusters of severe thunderstorms, in association with subsynoptic systems that cannot be explained by classical synoptic scale theory. The main criterion used to differentiate between the two types is the presence or absence of strong upper-level (500 mb or lower pressure) forcing. As explained in Palmén and Newton (1969), upper-level divergence is crucial

for extratropical cyclone development. Upper-level divergence is generally associated with positive vorticity advection (PVA) at 500 mb, and it is often not possible to find strong PVA in many tornado events, especially in the Great Plains.

Instead, as suggested by Tegtmeier (1974), many severe weather events occur with frontal waves that never complete the full life cycle of an extratropical cyclone. In this sense, they are "stable" frontal waves. There is also a growing body of evidence that such medium scale (subsynoptic) systems, which develop in zones of modest baroclinicity, play an important role in organizing severe convection. The numerical simulations of Gall (1976a,b), Nitta and Ogura (1972), Tokioka (1972) and Gambo (1970a) all suggest the disturbances, primarily confined to the lower troposphere, can develop on a subsynoptic time scale, independent of upper-level developments.

Instability theory, as developed by Stone (1966), Tokioka (1970), and Orlanski (1968), points out that in the range where Ro and Ri are of order unity, a variety of mechanisms can operate. Influential instabilities can be of Kelvin-Helmholtz (vertical shear), symmetric baroclinic, geostrophic baroclinic, or barotropic (horizontal shear) type. A small variation of either Ri or Ro can cause a large change in the theoretical growth rate for the various modes. Tokioka (1970) and Gall (1976a) point out that for classical baroclinic instability the growth rate increases for decreasing Ri, with the growth rate maximum shifting toward smaller wavelengths if the lapse rate increases under constant vertical shear. This is precisely the situation expected for frontal waves of the sort being considered. Also, Kung and Tsui (1975) and Gall (1976a) have shown that the primary source of subsynoptic scale kinetic energy production seems to be in baroclinic mode. Since the work of Kung and Tsui is observational, we tend to support the baroclinic instability hypothesis. Gambo (1970a) has shown that baroclinic instability becomes significant for Ri ~ 1, but emphasizes that other mechanisms, such as shearing instability, may also arise (Gambo, 1970b).

The numerical simulations of Tokioka (1972) and Nitta and Ogura (1972), as well as the observations of Matsumoto et al. (1970) have shown disturbances that are relatively cold (in the lower troposphere) on the south side of the system. However, Nitta and Ogura point out in their observations that the cold air is on the north side. The cases seen in this study also show cold air to the north. Thus, as proposed by Gall, the frontal wave circulation acts to decrease dynamic instability. In the absence of upper-level synoptic forcing, the warm air rising northward and the cold air sinking southward act to suppress further baroclinic development, via an increase of static stability and a decrease of vertical wind shear. It is anticipated that the severe convection developing in association with the subsynoptic wave plays a significant role in this process. The budget studies of McGinley (1973) support this hypothesis. His analysis of several cases, including two cases studied here, shows that when thunderstorms are present, subgrid heat sources and kinetic energy sinks exist at high levels, with heat sinks and kinetic energy sources at low levels. This indicates that severe convection acts to relieve conditions that allow the subsynoptic circulation to amplify.

In order to use the results obtained from band-pass filtering to shed light on the dynamics of subsyoptic systems, consider the vorticity (ζ) and divergence (δ) equations:

$$\frac{\partial \zeta}{\partial t} + \vec{V}\cdot\nabla(\zeta+f) + w\frac{\partial \zeta}{\partial z} = -(\zeta+f)\delta$$

$$+ \left(\frac{\partial w}{\partial y}\frac{\partial u}{\partial z} - \frac{\partial w}{\partial x}\frac{\partial v}{\partial z}\right) + \hat{k}\cdot(\nabla \times \vec{F} - \nabla\alpha \times \nabla p) \ , \qquad (37)$$

and

$$\frac{\partial \delta}{\partial t} + \vec{V}\cdot\nabla\delta + w\frac{\partial \delta}{\partial z} = -\delta^2 + f\zeta - \alpha\nabla^2 p + 2\hat{k}\cdot(\nabla u \times \nabla v) - \nabla\left(w\cdot\frac{\partial \vec{V}}{\partial z}\right) -$$

$$\nabla\alpha\cdot\nabla p + \nabla\cdot\vec{F} + \vec{V}\cdot(\hat{k} \times \nabla f) \ . \qquad (38)$$

These equations are to be applied only to the subsynoptic scale and, as mentioned before, are not intended to include the interaction terms with large scale flow.

There is no reliable way to calculate certain terms in (37) and (38) and these are omitted with the understanding that terms omitted are not necessarily considered negligible. Such terms include: those involving the vertical component of flow, any vertical derivative, or $\nabla\alpha$. Clearly, from surface data alone, no means of obtaining vertical motion or vertical derivatives exists without extremely restrictive assumptions. Baroclinic effects (terms involving $\nabla\alpha$) are non-negligible, as seen already, but the density variations across the grid are somewhat unreliable (as calculated from the observations); hence the omission at this time. Terms involving ∇f on the subsynoptic scale are negligible, as can be seen from our scale analysis, but these have been retained simply because of ease of calculation. The friction terms are also troublesome to calculate and so are omitted.

The remaining terms are calculated using the band-pass filtered fields in order to ascertain to what extent those effects we can estimate from surface data alone are important in the dynamics of the flow. After omitting the aforementioned terms in (37) and (38), it is found that

$$\frac{\partial \zeta}{\partial t} \sim -\vec{V}\cdot\nabla(\zeta+f) - (\zeta+f)\delta \ , \qquad (39)$$

and

$$\frac{\partial \delta}{\partial t} \sim -\vec{V}\cdot\nabla\delta - \delta^2 + f\zeta - \alpha\nabla^2 p + 2\hat{k}\cdot\nabla u \times \nabla v + \vec{V}\cdot(\hat{k} \times \nabla f) \ , \qquad (40)$$

where these are not necessarily equations, as noted. The extent to which (39) and (40) are satisfied as equalities, rather than associations (denoted by "~"), provides insight about the importance of the terms omitted.

Upon using the band-pass data to evaluate these equations, several remarkable results are found. First, relation (39) is found to be very nearly an equality. This agrees with the conclusions of Matsumoto et al. (1967) that on this scale, the vorticity distribution seems to be dominated by the divergence field. Thus, it appears that the vorticity of the subsynoptic system is generated by convergence and advection of already existing low-level vorticity. We find no significant need for a contribution from the tilting term, which disagrees with Matsumoto et al. (1967).

Scale analysis implies that the largest terms in (40) ought to be of order 10^{-8} s^{-2}. This is verified by the band-pass data, with the exception of the pressure Laplacian term ($-\alpha\nabla^2 p$), for which values are of order $10^{-7} s^{-2}$, in agreement with values obtained by Matsumoto and Ninomiya (1969). Eddy momentum transport is not clearly responsible for the apparent imbalance, as the pressure Laplacian remains the dominant term throughout the day. Subsynoptic scale momentum transport, implied by the terms

$$w \frac{\partial \delta}{\partial z} \text{ , } \nabla w \cdot \frac{\partial \vec{V}}{\partial z} \text{ , which are derived from } \nabla \cdot (w \frac{\partial \vec{V}}{\partial z})$$

is more likely to be responsible. Since the pressure term violates our preliminary scale analysis, such additional violations are not unreasonable. Note again that the pressure used here is already a sort of "perturbation pressure", since the low-pass pressure field had been subtracted out. Ageostrophic patterns seen in the low-pass fields reveal that the crossing-angle patterns are remarkably consistent from case to case and from one analysis time to another. This also suggests some relatively large scale, time independent effect which may be below the low-pass analysis scale, but of the same scale as the subsynoptic system. We cannot clearly isolate terms that balance the pressure Laplacian term. Nevertheless, if the pressure term is large compared to remaining terms and the effect is not temporally variant, then friction terms generated by small-scale eddies are probably not responsible for the balance, which has been proposed by Matsumoto et al. (1967).

Assuming that the pressure Laplacian term is, in fact, balanced by terms omitted from (40), a problem remains. Those terms of (40) that are retained after accounting for the balance still fail to explain the observed time variation of divergence. It is here that the temporal variation of the friction terms as a result of dry convection may play a role, as suggested by Sasaki (1973). The convergence seen immediately behind the dryline could be related to this effect, since convective mixing develops rapidly in the morning within the dry air as the morning inversion is eroded by solar heating.

In summary, it appears that the subsynoptic scale flow field satisfies a special type of "balance" equation with its mass field--namely

$$-\alpha\nabla^2 p = \nabla\cdot(w\,\frac{\partial\vec{V}}{\partial z}) \ . \qquad (41)$$

When this is satisfied, the observed time changes are at least of the same order as the remaining calculable terms in (40). If the friction term is assumed to be responsible for the residuals in the revised divergence equation, (40) becomes

$$\frac{\partial\delta}{\partial t} = -\vec{V}\cdot\nabla\delta - \delta^2 + f\zeta + 2\hat{k}\cdot\nabla u \times \nabla v + \vec{V}\cdot(\hat{k}\times\nabla f) + \nabla\cdot\vec{F} \ , \qquad (42)$$

where $\vec{F}$ is of the form $\partial/\partial z\ (\overline{u'w'})$.

The corresponding vorticity equation makes use of this special "balance" relation, since (41) implies

$$-\alpha\,\frac{\partial p}{\partial x} = w\,\frac{\partial u}{\partial z} \ , \qquad (43a)$$

$$-\alpha\,\frac{\partial p}{\partial y} = w\,\frac{\partial v}{\partial z} \ . \qquad (43b)$$

Neglecting horizontal gradients of vertical shear and of α, differentiating (43a) with respect to y and (43b) with respect to x gives the result that

$$\frac{\partial w}{\partial y}\frac{\partial u}{\partial z} - \frac{\partial w}{\partial x}\frac{\partial v}{\partial z} = -\alpha\left(\frac{\partial^2 p}{\partial x\partial y} - \frac{\partial^2 p}{\partial y\partial x}\right) = 0 \ .$$

This suggests that the tilting terms are negligible, and agrees well with the calculated results that imply (39) is an equality. Note also that the friction term appears unnecessary in (39) which agrees with the work of Matsumoto et al. (1967), in which frictional forces are considered irrotational. Thus, friction on this scale may be predominantly the result of eddy momentum transport, as postulated by Matsumoto et al.

6. SUMMARY AND RECOMMENDATIONS

We have developed a band-pass filter which can produce a detailed subsynoptic analysis from relatively noisy surface data. Analyses are well correlated with severe storm events when the organizing dynamical system is within the resolution limits imposed by the data.

From these results and available theoretical and numerical studies, a subsynoptic scale analysis is developed which is modified slightly for consistency with results using the band-pass data. This analysis suggests that anisentropic effects play a major role in subsynoptic events. Surface data are consistent with the hypothesis that the circulation is a low-level baroclinic instability phenomenon. These circulations can be detected well in

advance of thunderstorm development and appear to localize storm activity in such a way that very strong convection results, which may be instrumental in causing decay of this subsynoptic scale circulation. There is evidence that a subsynoptic scale balance exists between the pressure forces and the momentum transport generated by the vertical circulations of the subsynoptic system. This momentum transport may also influence the larger scale flow, creating characteristic patterns of ageostrophic winds.

To the author's knowledge, band-pass moisture divergence calculations have been done previously only by Hylton (1972). Hylton's method of computing moisture divergence differs somewhat from the method used in this study, so it is difficult to compare results. A method similar to band-pass filtering has been presented by Darkow and Livingston (1973) in which a Shuman (1957) filtered "low-pass" field is subtracted from the analyzed field, but no attempt at analysis of the spectral modification of this technique is made. Also, only pressure and static energy (Krietzberg, 1964) fields are analyzed, with no kinematic analysis.

Because of the lack of previous work in this area, a considerable effort could be made to use band-pass analysis in a wider range of cases. The work of Charba (1975) or Hudson (1971) has shown that "low-pass" moisture convergence has good correlation to severe weather events. Since this study substantiates their findings and indicates a possible extension to band-pass moisture convergence, this seems to be a fruitful avenue for further study. A question of some practical significance exists in this area--i.e., whether or not the results shown here can be useful in real-time forecasting. If this method can be applied on a real-time basis, not only is the range of test cases extended, but the method's usefulness for refining severe weather threat areas (as suggested by this post-storm study) can be evaluated.

Another potentially useful avenue of research is modeling the subsynoptic systems we have isolated with the band-pass filter. The results of the scale analysis provide a preliminary framework for additional numerical simulations. If one can successfully parameterize the anisentropic effects, the results shown can be applied to a simplified model, perhaps incorporating the implied balance equation as a diagnostic constraint. The role of diurnal effects in the dry air seem crucial to storm development, but it is not yet clear how the dryline (which is not a baroclinic zone) interacts with the frontal wave. This interaction could be clarified by numerical experiments.

Lack of knowledge of the subsynoptic scale vertical structure is a critical gap which inhibits further elucidation of subsynoptic processes. Available serial soundings in proximity to tornadic storms (Schaefer, personal communication) show deepening of the moist layer and erosion of the capping inversion prior to the onset of convection. This supports our hypothesis about the role of subsynoptic scale moisture convergence in localizing convection. Nevertheless, broader knowledge of the time variations of vertical stratification is needed to determine the validity of the suggestions about the dynamics of the subsynoptic system, especially in the dry air. Budget studies on the time and space scales considered could be fruitful in determination of the nature of energy conversions.

Examination of the problems inherent in meteorological analysis has shown the need to expand the theory of information content in our observations. This has a definite impact on the design of future experimental observation networks and data analysis methods. We need to ensure that our networks resolve the phenomena that we seek without excessive redundancy, for purely practical reasons. Any developing information theory has to account for the variety of physical mechanisms that can give rise to meteorological waves, and should also be able to account for non-uniform sampling networks.

Except possibly for surface observations, subsynoptic scale data are not likely to be available operationally in the foreseeable future, so motions on this scale must be examined as they interact with other scales. This analysis has suggested several possible interactions and it is likely that continuing research in the dynamics of these subsynoptic scales of motion will indicate more interactions. This scale, intermediate between the complex mesosystems seen in experimental data and the synoptic scale systems resolved by the standard large-scale observing system, probably plays an important intermediary role between the scales.

Subsynoptic systems represent an exciting area of study that is accessible with more or less conventional data. It is hoped that this work will stimulate further efforts to examine atmospheric processes on the subsynoptic scale.

7. ACKNOWLEDGEMENTS

The author wishes to express his sincere appreciation to those with whom many helpful discussions took place. These include Dr. Yoshi K. Sasaki of the University of Oklahoma, Drs. Edwin Kessler and Ronnie Alberty of the National Severe Storms Laboratory, and Dr. Joseph T. Schaefer of the Techniques Development Unit, National Severe Storms Forecast Center. A portion of this research was supported under NSF Grant No. GS 30976. Also, the typing help of Ms. Carol Cunningham (NSSL), Mrs. Deborah Killian (NSSL), and Ms. Deborah Barbieri (TDU) is gratefully acknowledged.

8. REFERENCES

Amble, O. (1953): "A Smoothing Technique for Pressure Maps", Bulletin, Amer. Meteor. Soc., 34, pp. 293-297.

Barnes, S. L. (1964): "A Technique for Maximizing Details in Numerical Weather Map Analysis", Jour. of Appl. Meteor., 3, pp. 396-409.

Barnes, S. L. (1973): "Mesoscale Objective Map Analysis Using Weighted Time-Series Observations", NOAA Tech. Memo. ERL NSSL-62, Norman, Nat. Severe Storms Lab., 60 pp.

Blackman, R. B., and J. N. Tukey (1958): The Measurement of Power Spectra (from the Point of View of Communications Engineering), New York: Dover Publications, 190 pp.

Charba, J. P. (1975): "Operational Scheme for Short Range Forecasts of Severe Local Weather", Preprints, Ninth Conf. on Severe Local Storms, Norman, Oklahoma, pp. 51-57.

Charney, J. G., and A. Eliassen. (1964): "On the Growth of the Hurricane Depression," Jour. of the Atmos. Sci., 21, pp. 68-75.

Darkow, G. L., and R. L. Livingston. (1973): "Hourly Surface Static Energy Analysis as a Delineator of Thunderstorm Outflow areas", Preprints, Eighth Conf. on Severe Local Storms, Denver, Colorado, pp. 232-237.

Fritsch, J. M. (1975): "Synoptic-Meso Scale Budget Relationships for a Tornado Producing Squall Line," Preprints, Ninth Conf. on Severe Local Storms, Norman, Oklahoma, pp. 165-172.

Gall, R. (1976a): "A Comparison of Linear Baroclinic Instability Theory with the Eddy Statistics of a General Circulation Model," Jour. of the Atmos. Sci., 33, pp. 349-373.

Gall, R. (1976b): "Structural Changes of Growing Baroclinic Waves," Jour. of the Atmos. Sci., 33, pp. 374-390.

Gambo, K. (1970a): "The Characteristic Feature of Medium-Scale Disturbances in the Atmosphere (I)," Jour. of the Meteor. Society of Japan, Ser. II, 48, pp. 173-184.

Gambo, K. (1970b): "The Characteristic Feature of Medium-Scale Disturbances in the Atmosphere (II)," Jour. of the Meteor. Society of Japan, Ser. II, 48, pp. 314-330.

Gandin, L. S. (1963): "Objective Analysis of Meteorological Fields," (English Translation, 1965): Program for Scientific Translations, Jerusalem, Israel, 242 pp.

Haltiner, G. J. (1971): Numerical Weather Prediction. New York: John Wiley, 317 pp.

Haurwitz, B. (1947): "Comments on the Sea-breeze Circulation," Jour. of Meteor., 4, pp. 1-8.

Hudson, H. R. (1971): "On the Relationship Between Horizontal Moisture Convergence and Convection Cloud Formation," Journal of Appl. Meteor., 10, pp. 755-762.

Hylton, D. A. (1972): "The Application of Low-Pass and Band-Pass Filtering Techniques to Surface and Upper Air Wind Fields," Master's Thesis, University of Oklahoma, Norman, Oklahoma, 87 pp.

Krietzberg, C. W. (1964): "The Structure of Occlusions as Determined from Serial Ascents and Vertically Directed Radar," Air Force Cambridge Research Laboratory, Research Report 64-26, Cambridge, Massachusetts, 121 pp.

Kung, E. C., and T. L. Tsui. (1975): "Subsynoptic-Scale Kinetic Energy Balance in the Storm Area," Jour. of the Atmos. Sci., 32, pp. 729-740.

Lewis, J. M. (1971): "Variational Subsynoptic Analysis with Applications to Severe Local Storms," Mon. Wea. Rev., 99, pp. 786-795.

Lumley, J. L., and H. A. Panofsky. (1964): The Structure of Atmospheric Turbulence. New York: John Wiley Interscience, 239 pp.

Maddox, R. A., and W. M. Gray. (1973): "A Frictionally Driven Model for Tornado Genesis with Similarities to Hurricane Genesis," Preprints, Eighth Conference on Severe Local Storms, Denver, Colorado, pp. 203-206.

Matsumoto, S., and K. N. Ninomiya. (1969): "On the Role of Convective Momentum Exchange in the Mesoscale Gravity Wave," Jour. of the Meteor. Soc. of Japan, Ser. II, 47, pp. 75-85.

Matsumoto, S., K. N. Ninomiya, and T. Akiyama. (1967): "A Synoptic and Dynamic Study of the Three-Dimensional Structure of Mesoscale Disturbances Observed in the Vicinity of A Cold Vortex Center," Jour. of the Meteor. Society of Japan, Ser. II, 45, pp. 64-82.

Matsumoto, S., S. Yoshizumi, and M. Takeuchi. (1970): "On the structure of the 'Baiu-Front' and the Associated Intermediate Scale Disturbances in the Low Atmospnere", Jour. of the Meteor. Society of Japan, Ser. II, 48, pp. 479-491.

McFarland, M. J. (1975): "Sasaki's Variational Optimization Analysis of Temperature and Moisture Advection in a Severe Storm Environment," Preprints, Ninth Conference on Severe Local Storms, Norman, Oklahoma, pp. 158-164.

McGinley, J. A. (1973): "Environmental Energy Fields Associated With Severe Storms," Master's Thesis, University of Oklahoma, Norman, Oklahoma, 129 pp.

McGinley, J. A., and Y. K. Sasaki. (1975): "The Role of Symmetric Instabilities in Thunderstorm Development on Drylines," Preprints, Ninth Conf. on Severe Local Storms, Norman, Oklahoma, pp. 173-180.

Miller, R. C. (1972): "Notes on Analysis and Severe-Storm Forecasting Procedures of the Air Force Global Weather Central," Air Weather Service Technical Report 200 (Rev.), Air Weather Service, Scott Air Force Base, Illinois, approximately 190 pp.

Nitta, T., and Y. Ogura. (1972): "Numerical Simulation of the Development of the Intermediate-Scale Cyclone in a Moist Atmosphere," Jour. of the Atmos. Sci., 29, pp. 1011-1024.

Orlanski, I. (1968): "Instability of Frontal Waves," Jour. of the Atmos. Sci., 25, pp. 178-200.

Ostby, F. P., Jr. (1975): "An Application of Severe Storm Forecast Techniques to the Outbreak of June 8, 1974," Preprints, Ninth Conference on Severe Local Storms, Norman, Oklahoma, pp. 7-12.

Palmén, E., and C. W. Newton. (1969): Atmospheric Circulation Systems. New York: Academic Press, International Geophysics Series, 13, 603 pp.

Sasaki, Y. (1958): "An Objective Analysis Based on the Variational Method," Jour. of the Meteor. Society of Japan, Ser. II, 36, pp. 77-88.

Sasaki, Y. (1960): "An Objective Analysis for Determining Initial Conditions for the Primitive Equations," Technical Report Project 208, Texas A&M University, College Station, Texas, 22 pp.

Sasaki, Y. (1970): "Some Basic Formalisms in Numerical Variational Analysis," Mon. Weather Review, 98, pp. 875-883.

Sasaki, Y. (1973): "Mechanism of Squall-Line Formation as Suggested from Variational Analysis of Hourly Surface Observations," Preprints, Eighth Conference on Severe Local Storms, Denver, Colorado, pp. 300-307.

Schaefer, J. T. (1973): "The Motion and Morphology of the Dryline," NOAA Technical Memorandum ERL NSSL-66, Norman, Oklahoma, 81 pp.

Schaefer, J. T. (1974): "The Environment Near the Dryline," Proceedings, Opening Meeting for SESAME, Boulder, Colorado, (Published 1975), pp. 206-216.

Schaefer, J. T. (1976): "Moisture Features of the Convective Boundary Layer in Oklahoma", Quart. Jour. of the Roy. Meteor. Soc., 102, pp. 447-451.

Seibers, J. O., F. Hidalgo, S. A. Tegtmeier, and M. Young. (1975): "Guide for Using GOES/SMS Imagery in Severe Weather Forecasting," USAFETAC, Andrews Air Force Base, Maryland, 56 pp.

Sheets, R. C. (1973): "Analysis of STORMFURY Data Using The Variational Optimization Approach," NOAA Technical Report, ERL 264-WMPO 1, Boulder, Colorado, 92 pp.

Shuman, F. G. (1957): "Numerical Methods in Weather Prediction: II Smoothing and Filtering," Mon. Wea. Rev., 85, pp. 357-361.

Stephens, J. J. (1971): "On Definable Scale Reduction by Simultaneous Observations," Jour. of Appl. Meteor., 10, pp. 23-25.

Stone, P. (1966): "On Non-Geostrophic Baroclinic Instability," Jour. of the Atmos. Sci., 23, pp. 390-400.

Tegtmeier, S. A. (1974): "The Role of the Surface, Subsynoptic, Low Pressure System in Severe Weather Forecasting," Master's Thesis, University of Oklahoma, Norman, Oklahoma, 66 pp.

Tokioka, T. (1970): "Non-Geostrophic and Non-Hydrostatic Stability of a Baroclinic Fluid", Jour. of the Meteor. Society of Japan, Ser. II, 48, pp. 503-520.

Tokioka, T. (1972): "A Numerical Experiment of Medium-Scale Disturbances: Dry Model", Jour. of the Meteor. Society of Japan, Ser. II, 50, pp. 259-270.

Wu, S. S. (1965): "A Study of Heat Transfer Coefficients in the Lowest 400 meters of the Atmosphere", Jour. of Geophys. Res., 70, pp. 1801-1807.

NATIONAL SEVERE STORMS LABORATORY

The NSSL Technical Memorandum, beginning with No. 28, continue the sequence established by the U. S. Weather Bureau National Severe Storms Project, Kansas City, Missouri. Numbers 1-22 were designated NSSP Reports. Numbers 23-27 were NSSL Reports, and 24-27 appeared as subseries of Weather Bureau Technical Notes. These reports are available from the National Technical Information Service, Operations Division, Springfield, Virginia 22151, for $3.00 and a microfiche version for $0.95. NTIS numbers are given below in parentheses.

No. 1 National Severe Storms Project Objectives and Basic Design. Staff, NSSP. March 1961. (PB-168207)

No. 2 The Development of Aircraft Investigations of Squall Lines from 1956-1960. B. B. Goddard. (PB-168208)

No. 3 Instability Lines and Their Environments as Shown by Aircraft Soundings and Quasi-Horizontal Traverses. D. T. Williams. February 1962. (PB-168209)

No. 4 On the Mechanics of the Tornado. J. R. Fulks. February 1962. (PB-168210)

No. 5 A Summary of Field Operations and Data Collection by the National Severe Storms Project in Spring 1961. J. T. Lee. March 1962. (PB-165095)

No. 6 Index to the NSSP Surface Network. T. Fujita. April 1962. (PB-168212)

No. 7 The Vertical Structure of Three Dry Lines as Revealed by Aircraft Traverses. E. L. McGuire. April 1962. (PB-168213)

No. 8 Radar Observations of a Tornado Thunderstorm in Vertical Section. Ralph J. Donaldson, Jr. April 1962. (PB-174859)

No. 9 Dynamics of Severe Convective Storms. Chester W. Newton. July 1962. (PB-163319)

No. 10 Some Measured Characteristics of Severe Storms Turbulence. Roy Steiner and Richard H. Rhyne. July 1962. (N62-16401)

No. 11 A Study of the Kinematic Properties of Certain Small-Scale Systems. D. T. Williams. October 1962. (PB-168216)

No. 12 Analysis of the Severe Weather Factor in Automatic Control of Air Route Traffic. W. Boynton Beckwith. December 1962. (PB-168217)

No. 13 500-Kc./Sec. Sferics Studies in Severe Storms. Douglas A. Kohl and John E. Miller. April 1963. (PB-168218)

No. 14 Field Operations of the National Severe Storms Project in Spring 1962. L. D. Sanders. May 1963. (PB-168219)

No. 15 Penetrations of Thunderstorms by an Aircraft Flying at Supersonic Speeds. G. P. Roys. Radar Photographs and Gust Loads in Three Storms of 1961 Rough Rider. Paul W. J. Schumacher. May 1963. (PB-168220)

No. 16 Analysis of Selected Aircraft Data from NSSP Operations, 1962. T. Fujita. May 1963. (PB-168221)

No. 17 Analysis of Methods for Small-Scale Surface Network Data. D. T. Williams. August 1963. (PB-168222)

No. 18 The Thunderstorm Wake of May 4, 1961. D. T. Williams. August 1963. (PB-168223)

No. 19 Measurements by Aircraft of Condensed Water in Great Plains Thunderstorms. George P. Roys and Edwin Kessler. July 1966. (PB-173048)

No. 20 Field Operations of the National Severe Storms Project in Spring 1963. J. T. Lee, L. D. Sanders, and D. T. Williams. January 1964. (PB-168224)

No. 21 On the Motion and Predictability of Convective Systems as Related to the Upper Winds in a Case of Small Turning of Wind with Height. James C. Fankhauser. January 1964. (PB-168225)

No. 22 Movement and Development Patterns of Convective Storms and Forecasting the Probability of Storm Passage at a Given Location. Chester W. Newton and James C. Fankhauser. January 1964. (PB-168226)

No. 23 Purposes and Programs of the National Severe Storms Laboratory, Norman, Oklahoma. Edwin Kessler. December 1964. (PB-166675)

No. 24 Papers on Weather Radar, Atmospheric Turbulence, Sferics, and Data Processing. August 1965. (AD-621586)

No. 25 A Comparison of Kinematically Computed Precipitation with Observed Convective Rainfall. James C. Fankhauser. September 1965. (PB-168445)

No. 26 Probing Air Motion by Doppler Analysis of Radar Clear Air Returns. Roger M. Lhermitte. May 1966. (PB-170636)

No. 27 Statistical Properties of Radar Echo Patterns and the Radar Echo Process. Larry Armijo. May 1966. The Role of the Kutta-Joukowski Force in Cloud Systems with Circulation. J. L. Goldman. May 1966. (PB-170756)

No. 28 Movement and Predictability of Radar Echoes. James Warren Wilson. November 1966. (PB-173972)

No. 29 Notes on Thunderstorm Motions, Heights, and Circulations. T. W. Harrold, W. T. Roach, and Kenneth E. Wilk. November 1966. (AD-644899)

No. 30 Turbulence in Clear Air Near Thunderstorms. Anne Burns, Terence W. Harrold, Jack Burnham, and Clifford S. Spavins. December 1966. (PB-173992)

No. 31 Study of a Left-Moving Thunderstorm of 23 April 1964. George R. Hammond. April 1967. (PB-174681)

No. 32 Thunderstorm Circulations and Turbulence from Aircraft and Radar Data. James C. Fankhauser and J. T. Lee. April 1967. (PB-174860)

No. 33 On the Continuity of Water Substance. Edwin Kessler. April 1967. (PB-175840)

No. 34 Note on the Probing Balloon Motion by Doppler Radar. Roger M. Lhermitte. July 1967. (PB-175930)

No. 35 A Theory for the Determination of Wind and Precipitation Velocities with Doppler Radars. Larry Armijo. August 1967. (PB-176376)

No. 36 A Preliminary Evaluation of the F-100 Rough Rider Turbulence Measurement System. U. O. Lappe. October 1967. (PB-177037)

No. 37 Preliminary Quantitative Analysis of Airborne Weather Radar. Lester P. Merritt. December 1967. (PB-177188)

No. 38 On the Source of Thunderstorm Rotation. Stanley L. Barnes. March 1968. (PB-178990)

No. 39 Thunderstorm - Environment Interactions Revealed by Chaff Trajectories in the Mid-Troposphere. James C. Fankhauser. June 1968. (PB-179659)

No. 40 Objective Detection and Correction of Errors in Radiosonde Data. Rex L. Inman. June 1968. (PB-180284)

No. 41 Structure and Movement of the Severe Thunderstorms of 3 April 1964 as Revealed from Radar and Surface Mesonetwork Data Analysis. Jess Charba and Yoshikazu Sasaki. October 1968. (PB-183310)

No. 42 A Rainfall Rate Sensor. Brian E. Morgan. November 1968. (PB-183979)

No. 43 Detection and Presentation of Severe Thunderstorms by Airborne and Ground-Based Radars: A Comparative Study. Kenneth E. Wilk, John K. Carter, and J. T. Dooley. February 1969. (PB-183572)

No. 44 A Study of a Severe Local Storm of 16 April 1967. George Thomas Haglund. May 1969. (PB-184970)

No. 45 On the Relationship Between Horizontal Moisture Convergence and Convective Cloud Formation. Horace R. Hudson. March 1970. (PB-191720)

No. 46 Severe Thunderstorm Radar Echo Motion and Related Weather Events Hazardous to Aviation Operations. Peter A. Barclay and Kenneth E. Wilk. June 1970. (PB-192498)

No. 47 Evaluation of Roughness Lengths at the NSSL-WKY Meteorological Tower. Leslie D. Sanders and Allen H. Weber. August 1970. (PB-194587)

No. 48 Behavior of Winds in the Lowest 1500 ft in Central Oklahoma: June 1966-May 1967. Kenneth C. Crawford and Horace R. Hudson. August 1970.

No. 49 Tornado Incidence Maps. Arnold Court. August 1970. (COM-71-00019)

No. 50 The Meteorologically Instrumented WKY-TV Tower Facility. John K. Carter. September 1970. (COM-71-00108)

No. 51 Papers on Operational Objective Analysis Schemes at the National Severe Storms Forecast Center. Rex L. Inman. November 1970. (COM-71-00136)

No. 52 The Exploration of Certain Features of Tornado Dynamics Using a Laboratory Model. Neil B. Ward. November 1970. (COM-71-00139)

No. 53 Rawinsonde Observation and Processing Techniques at the National Severe Storms Laboratory. Stanley L. Barnes, James H. Henderson, and Robert J. Ketchum. April 1971. (COM-71-00707)

No. 54 Model of Precipitation and Vertical Air Currents. Edwin Kessler and William C. Bumgarner. June 1971. (COM-71-00911)

No. 55 The NSSL Surface Network and Observations of Hazardous Wind Gusts. Operations Staff. June 1971. (COM-71-00910)

No. 56 Pilot Chaff Project at the National Severe Storms Laboratory. Edward A. Jessup. November 1971. (COM-72-10106)

No. 57 Numerical Simulation of Convective Vortices. Robert P. Davies-Jones and Glenn T. Vickers. November 1971. (COM-72-10269).

No. 58 The Thermal Structure of the Lowest Half Kilometer in Central Oklahoma: December 9, 1966-May 31, 1967. R. Craig Goff and Horace R. Hudson. July 1972. (COM-72-11281)

No. 59 Cloud-to-Ground Lightning Versus Radar Reflectivity in Oklahoma Thunderstorms. Gilbert D. Kinzer. September 1972. (COM-73-10050)

No. 60 Simulated Real Time Displays of Velocity Fields by Doppler Radar. L. D. Hennington and G. B. Walker. November 1972. (COM-73-10515)

No. 61 Gravity Current Model Applied to Analysis of Squall-Line Gust Front. Jess Charba. November 1972. (COM-73-10410)

No. 62 Mesoscale Objective Map Analysis Using Weighted Time-Series Observations. Stanley L. Barnes. March 1973. (COM-73-10781)

No. 63 Observations of Severe Storms on 26 and 28 April 1971. Charles L. Vlcek. April 1973. (COM-73-11200)

No. 64 Meteorological Radar Signal Intensity Estimation. Dale Sirmans and R. J. Doviak. September 1973. (COM-73-11923/2AS)

No. 65 Radiosonde Altitude Measurement Using Double Radiotheodolite Techniques. Stephan P. Nelson. September 1973. (COM-73-11934/9AS)

No. 66 The Motion and Morphology of the Dryline. Joseph T. Schaefer. September 1973. (COM-74-10043)

No. 67 Radar Rainfall Pattern Optimizing Technique. Edward A. Brandes. March 1974.

No. 68 The NSSL/WKY-TV Tower Data Collection Program: April-July 1972. R. Craig Goff and W. David Zittel. May 1974.

No. 69 Papers on Oklahoma Thunderstorms, April 29-30, 1970. Stanley L. Barnes, Editor. May 1974.

No. 70 Life Cycle of Florida Key's Waterspouts. Joseph H. Golden. June 1974.

No. 71 Interaction of Two Convective Scales Within a Severe Thunderstorm: A Case Study and Thunderstorm Wake Vortex Structure and Aerodynamic Origin. Leslie R. Lemon. June 1974.

No. 72 Updraft Properties Deduced from Rawinsoundings. Robert P. Davies-Jones and James H. Henderson. October 1974.

No. 73 Severe Rainstorm at Enid, Oklahoma - October 10, 1973. L. P. Merritt, K. E. Wilk, and M. L. Weible. November 1974.

No. 74 Mesonetwork Array: Its Effect on Thunderstorm Flow Resolution. Stanley L. Barnes. October 1974.

No. 75 Thunderstorm-Outflow Kinematics and Dynamics. R. Craig Goff. December 1975.

No. 76 An Analysis of Weather Spectra Variance in a Tornadic Storm. Philippe Waldteufel. May 1976.

No. 77 Normalized Indices of Destruction and Deaths by Tornadoes. Edwin Kessler and J. T. Lee. June 1976.

No. 78 Objectives and Accomplishments of the NSSL 1975 Spring Program. K. Wilk, K. Gray, C. Clark, D. Sirmans, J. T. Dooley, J. Carter, and W. Bumgarner. July 1976.

☆ U.S. GOVERNMENT PRINTING OFFICE:1977—777-045 / 1222 REGION NO.8